

SMARTPHONE INTEGRATION AND FLUID FLOW CONTROL IN A
HAND-HELD MICROFLUIDIC LAB-ON-CHIP BIOSENSOR

BY

NICHOLAS M. DIFILIPPO

A THESIS SUBMITTED IN PARTIAL FULFILLMENT OF THE
REQUIREMENTS FOR THE DEGREE OF

MASTER OF SCIENCE

IN

MECHANICAL ENGINEERING AND APPLIED MECHANICS

UNIVERSITY OF RHODE ISLAND

2012

MASTER OF SCIENCE THESIS

OF

Nicholas M. DiFilippo

APPROVED:

Thesis Committee:

Major Professor Mohammed Faghri

Constantine Anagnostopoulos

William Ohley

Nasser H. Zawia

DEAN OF THE GRADUATE SCHOOL

UNIVERSITY OF RHODE ISLAND

2012

ABSTRACT

This experimental study investigates the possibility of creating two separate systems for a Point-of-Care (POC), Lab-on-a Chip (LOC) handheld biosensor for the detection of C-reactive protein (CRP). One of these systems is a fluid control system that would facilitate the automation of the pumping of liquid, for a test for CRP. This fluid control system would use a Charged Couple Device (CCD) as a way to monitor the detection site for any changes. The microfluidic system that is used is fabricated from Polydimethylsiloxane (PDMS) and is either bonded to another piece of PDMS or a thin glass base.

The second system that this research aims to create is a wireless system that could exhibit complete control over the handheld unit. This system will use a custom iPhone application (app) for the graphics user interface (GUI), and will be able to send data to start a test, as well as receive the results after the completion of a test. For the first time, a completely automated, reliable, and inexpensive fluid handling system will be presented. As will the ability for a smartphone to operate a handheld microfluidic device test for CRP.

ACKNOWLEDGEMENTS

I would like to take the opportunity to thank my major advisor Dr. Mohammad Faghri for introducing me to the field of microfluidics and his continued support throughout this project. I would like to thank Dr. Constantine Anagnostopoulos for all the suggestions and guidance he offered throughout the course of this project whenever a question arose.

I would especially like to thank John Jones for all of the help and guidance that he gave me throughout our time working together. His patience in teaching and explaining different concepts in various disciplines ranging from Electrical Engineering to Biology was truly inspiring.

I would also like to thank Tom DeRensis, who volunteered his time and was helpful with coding various aspects of this project and my colleagues in the microfluidic group Dr. Toru Yamada, Dr. Hong Chen, Manuel Muller, Jeremy Cogswell, Mike Godfrin, and Mike Franzblau. I would also like to take this opportunity to recognize my family especially my brother Mark DiFilippo. Without their help, love, and support it would not have been possible for me to complete this project.

TABLE OF CONTENTS

ABSTRACT	ii
ACKNOWLEDGEMENTS	iii
TABLE OF CONTENTS.....	iv
LIST OF TABLES	vi
LIST OF FIGURES	vii
CHAPTER 1 – INTRODUCTION	1
1.1 Microfluidics and Point-of-Care	1
1.2 Fluid Control Overview	2
1.3 Connectivity in Medical Devices Overview.....	2
1.4 Motivation.....	3
1.5 Statement of the Problem	4
1.6 Objective	4
CHAPTER 2 – BACKGROUND AND REVIEW OF LITERATURE.....	6
2.1 Fluid Flow Control	6
2.1.1 Passive Control.....	6
2.1.2 Active Control	7
2.1.3 CCD Imagers.....	8
2.1.4 Filter Requirements	10
2.1.5 Biology	12
2.1.6 Edge Detection.....	14
2.2 Smartphone Integration	15
2.2.1 Network Background	15
2.2.2 Wireless overview in Medical Devices	18
2.2.3 Competing Point of Care Devices	20
CHAPTER 3 - METHODOLOGY.....	23
3.1 Fluid Handling.....	23

3.1.1 Determination of Bayer Pattern	23
3.1.2 Initial Fluid Handling Setup	25
3.1.3 Final Fluid Handling Setup.....	26
3.1.4 Change of Design of Microfluidic Chip	28
3.1.5 Edge Detection Methodology	32
3.1.6 Feedback Control Methodology	38
3.2 Smartphone and Network Integration.....	42
3.2.1 Arduino and Shield	42
3.2.2 Environments	44
3.2.3 Network	44
CHAPTER 4 – FINDINGS	47
4.1 Fluid Flow Control	47
4.1.1 Edge Detection with air in channels	47
4.1.2 Edge Detection with Liquid in Channels.....	49
4.1.3 LED and Filter Parameters	54
4.1.4 Height and Voltage of LED.....	59
4.1.5 Feedback Pumping.....	61
4.2 Smartphone Integration	68
4.2.1 Microcontroller Prototypes.....	68
4.2.2 Smartphone Applications.....	70
4.2.3 Network Integration.....	74
4.2.4 Preliminary Communication for a Completely Wireless Unit	75
CHAPTER 5 - CONCLUSION	78
5.1 Conclusions	78
5.2 Future Work	78
NOMENCLATURE.....	81
BIBLIOGRAPHY	83

LIST OF TABLES

TABLE	PAGE
Table 1: Blue Pixels	24
Table 2: Red Pixels	24
Table 3: Green Pixels	24
Table 4: Bayer Pattern.....	36
Table 5: List of programming environments.....	44
Table 6: List of different LED parameters	54
Table 7: List of different filters and specifications	55
Table 8: Results of using different LEDs with different filters	58
Table 9: Results of Voltages and Heights for the Flat Amber LED	60
Table 10: Results of Voltages and Heights for the White LED	60
Table 11: Results for determining volumetric flow rate	65

LIST OF FIGURES

FIGURE	PAGE
Figure 1: Spectral Sensitivity of FireI CCD	10
Figure 2: Longpass filter specification from Edmunds Optics	11
Figure 3: Shortpass Filter	12
Figure 4: Bandpass filter specifications from Edmunds Optics	12
Figure 5. Sandwich assay protocol for detection of C-reactive protein in buffer solution.....	13
Figure 6: 1D representation of edge detection taken from Handbook of Image and Video Processing p. 536.	14
Figure 7: Internal vs. External IP Address	17
Figure 8: Server Client Representation	18
Figure 9: Bayer Pattern of CCD Imager	25
Figure 10: Optical Detection Setup	26
Figure 11: Close up view showing glass slide inserted into stage.....	26
Figure 12: Final Setup for fluid control	27
Figure 13: Sequentially Loaded Chip	28
Figure 14: Original Elliptical Chip	28
Figure 15: Region of interest placed in the elliptical detection chamber.....	29
Figure 16: Image of elliptical detection chamber with a) air and with b) liquid.....	29
Figure 17: New 'S' Channel design.....	31

Figure 18: Image of Calibration and ‘S’ channel detection chamber a) with air and b) with liquid	31
Figure 19: Channels with air in liquid in the detection site along with a 3d histogram on the image	32
Figure 20: Raw data of image; Black are blue pixels, Gray are Green Pixels, White are Red.....	33
Figure 21: Channel Coordinate Transformation.....	37
Figure 22: Feedback Controller Logic	41
Figure 23: Arduino Nano Mega 2560 by Emartee	43
Figure 24: Copperhead Wifi Shield	43
Figure 25: Wireless handheld Communication	46
Figure 26: MATLAB Image Detection Methods a) Sobel b) Prewitt c) Roberts d) Log e) Zerocross f) Canny	47
Figure 27: ROI of interest of different edge detection methods with air in channel	48
Figure 28: Region of Interest with air in channels over various days	49
Figure 29: ROI of different edge detection methods with liquid in channel.....	51
Figure 30: Binary Image with new Edge Detection and Region of Interest	52
Figure 31: Region of Interest placement finding all edges	53
Figure 32: Region of interest Placement using absolute positioning.....	54
Figure 33: Transmission vs. Wavelength for Wratten 12 Filter	56
Figure 34: Results for Cool White LED with various filters	57
Figure 35: Flat Amber LED with different Filters.....	58
Figure 36: Image results for white LED at various voltages and heights	61

Figure 37: Manual Pumping with half second delay	62
Figure 38: Pumping with Bartels Micropump.....	63
Figure 39: Dimensions of the 'S' channel 0.25mm height.....	64
Figure 40: Different geometric chip design (depth 0.25mm).....	66
Figure 41: Serum in Feedback Loop.....	67
Figure 42: Whole Blood in Detection Channel	67
Figure 43: Quantum Dots in Detection Channel	68
Figure 44: List of different Fluid that work with feedback control	68
Figure 45: Initial handheld unit prototype.....	69
Figure 46: Final Microcontroller and modifications.....	69
Figure 47: Prototype of the Handheld unit.....	70
Figure 48: First generation of smartphone app on iPhone	71
Figure 49: Second Generation of smartphone app on Android	72
Figure 50: Third and Final Generation of smartphone app on iPhone	74
Figure 51: Time taken to send bytes wirelessly from microcontroller	76
Figure 52: Fez Cobra.....	76
Figure 53: Proposed Network Communication for a completely wireless unit	77

CHAPTER 1 – INTRODUCTION

1.1 Microfluidics and Point-of-Care

Microfluidics is the science of the manipulation of liquid on a small scale (usually sub millimeter). Microfluids, unlike fluids at the macroscopic level are, dominated by laminar flows, surface tension, and capillary forces rather than atmospheric pressure and gravity. This is a growing area that can solve some issues that arise from current diagnostic tests. Some advantages of microfluidic systems are the small sample sizes and reagents required, and the ability to achieve fast and accurate results [1, 2, 3].

These advantages could lead to a decrease in the overall cost of tests, and faster more reliable diagnoses [4]. The integration of wireless communication could lead to new devices and instruments, [5] and faster integration to a patient's record [6]. Lab-on-a-Chip (LOC) technology can also be used to monitor health in developing countries. In these resource poor settings, it is imperative that the tests be simple to use, inexpensive, and capable of delivering fast and accurate results [7, 8, 9].

In today's society, there is a market for easy to use, low cost, fast, and reliable Point-of-Care (POC) devices. Currently, one way to perform diagnostic tests is to use permanent integrated instruments. These instruments are usually very big, expensive, and are located in a centralized lab where the samples that need to be analyzed are sent. Another way to perform a diagnostic test is to use disposable tests (lateral flow strips), or disposable tests with a reader. Disposable tests have been used for about the past fifteen years. These test strips are typically inexpensive, and can be stored for a

long period of time. However, the end results are limited to either a 'yes' or 'no', which might not be satisfactory in certain situations [10].

1.2 Fluid Control Overview

Fluid control in microfluidics is normally performed by active or passive microfluidic control schemes. Some of the benefits of passive controls are they are inexpensive, and do not require external power or external components. Unfortunately, one of the drawbacks is that there is no guarantee that the reagents will be at the appropriate place at the appropriate time and these systems are designed to be very application specific.

Active controls are another method of controlling fluid flow. A benefit that active controls have over passive controls is their ability to exhibit better control over the fluid. Some drawbacks of active controls include a high cost, complex circuitry, and the need for external components [11].

1.3 Connectivity in Medical Devices Overview

As access to wireless connectivity continues to increase, more and more devices will begin to incorporate wireless capabilities. Medical devices are no exception, and some medical devices have already been produced that take advantage of this emerging technology. A smart medication system that can remind people to take their medications at certain times, and various sensors that can be worn to collect real time data of vital signs or physiological data have already been produced [12, 13]. Research groups, such as the West Wireless Health Institute and Harvard's research

group CodeBlue, are devoted to creating and developing applications for wireless sensor technology in medical devices and the medical field.

1.4 Motivation

Previously, the Affordable-Point-of-Care Immunoassay System (APOCIS) designed by the University of Rhode Island (URI) employed a micropump and three-way magnetically latched solenoid valve to control the liquid. It was initially desired to pump the fluid throughout the entire test using a passive control scheme, but it was not possible to obtain a flow rate slow enough with the Bartels micropump that was used. Therefore, the sequential loading of the reagents in the APOCIS device was solely based on a timing mechanism. Due to the unreliability of the micropump, it was not possible to get repeatable results. Occasionally, the pump would shut off before the reagents would reach the detection chamber or after they had passed. This is a problem that needs to be addressed for the creation of an automated handheld POC system. Additionally, an operator had to be alert during the test in order to push a button on a computer to capture the results when the blue Light Emitting Diode (LED) was on.

The motivation of this research is to improve upon the previous APOCIS device and create a wireless handheld microfluidic device that will be capable of performing an automated test for C-reactive protein (CRP). CRP is a biomarker that can be used to indicate inflammation of muscles that could be a precursor to a heart attack. Both the smartphone integration and the fluid flow control are important aspects that are needed for a completely automated test. The smartphone app will act as a graphics user interface (GUI) so that the only actions a user has to perform is to

insert a microfluidic cartridge into the device, and press “Start Test” on the iPhone.

The fluid control method that is used will improve upon the timing and accuracy of the sequential loading in the handheld microfluidic unit.

1.5 Statement of the Problem

The proposed research will focus on two problems dealing with the fabrication of a handheld device for POC diagnostics.

The first problem consists of a way to precisely control the flow of fluid in micro channels. Using the main detection system of the handheld device, a lensless charge-coupled device (CCD), it is possible to determine if there is air or fluid in the detection chamber of a microfluidic chip. By using this information, it will be possible to stop and start a micro-pump or other pumping methods for increased reliability.

The second problem consists of the integration of wireless control to the handheld POC system. The wireless capabilities will allow the handheld system to be able to be controlled through a smartphone app (App) and have the ability to communicate with other devices. The proposed system will allow for the automation of a test for CRP from a drop of blood, and for the results of the test to be delivered to the smartphone app, or healthcare provider, via e-mail.

1.6 Objective

The objective of this research is to create two different systems for a handheld microfluidic device that will improve upon the APOCIS unit. One of these systems, the fluid handling system, should utilize feedback control using images taken by a CCD imager. Comparison of these images will be used to determine whether liquid or

air is in the detection chamber and whether the pump should be on or off. This method of fluid control will be more accurate than the previous method based off timing used in the APOCIS unit. By using a CCD imager to look at various areas of detection site, it would be possible to create a novel technique for fluid control that would determine if there was liquid or air in the chamber.

The second system consists of the integration of network capabilities to the handheld device. A smartphone app that has the ability to control the handheld microfluidic system will be created. Eventually, the smartphone app would be the only user interface on the device needed to be capable of sending information to a server and receiving the results of a test. On the APOCIS device, the fluorometer had to be connected to a computer and an operator had to be alert during the test in order to capture the data at the appropriate time. This test will be completely automated with the results delivered via email and to a smartphone.

CHAPTER 2 – BACKGROUND AND REVIEW OF LITERATURE

2.1 Fluid Flow Control

2.1.1 Passive Control

Passive fluid control is an inexpensive way of controlling fluid flow by taking advantage of natural forces that occur on the microscale. Typically, passive control schemes consist of mixers [14, 15], valves [16, 17], and passive actuation schemes [18, 19]. Another means of passive fluid control is pumping the fluid very slowly, which allows the fluid to be continuously pumped throughout an entire test [9, 20].

Passives valves can be used as pressure barriers that can stop a fluid until a force that exceeds the pressure of the barrier has been built up. Other methods of passive control include lining the channel walls with absorbable salt that would alter the fluid flow or shortening the channel dimensions to slow down the liquid [17].

Another passive control scheme presented by Walker et al [19] uses the surface energy that is present in a small drop of liquid. By having two ports, a larger reservoir port and a smaller pumping port, a pressure differential is obtained. If a large drop of water is placed on the reservoir port, the pressure at the port becomes zero. Then if a smaller drop is placed on the pumping port, a higher pressure will be created over that port. The resulting pressure gradient that is created causes the fluid to flow towards the reservoir port.

2.1.2 Active Control

Fluid manipulation using active control schemes, are more accurate than using passive controls. The equipment needed to use active controls, usually make these methods of fluid control more expensive. Some examples of active controls include mechanical valves, such as torque valves [21], electrokinetic valves [22], and pneumatic valves [23].

A torque valve presented by Weibel et al [21] is an inexpensive way to control fluid flow since it consists of a machine screw that is driven into the micro channel; however it needs to be activated by a user, which would not be ideal for an automated test. An electrokinetic valve acts like a router of the fluid and is well suited for continuous flow because fluids can quickly be switched between channels. The only downfall is that the micropump used in the device is not capable of producing such low flow rates [24].

A monolithic valve presented by Unger et al [25], is fabricated from a single type of material, and when pneumatically actuated, the membranes are deflected down into the channel impeding the fluid flow. These valves require the channel geometry to consist of a round cross section in order to work properly. Channel geometries that have rectangular or trapezoidal cross sections are not closed completely. Accurate control of the fluid can be obtained by varying the pressures applied to the control line.

Microspheres could also be used as active control because when they are heated, their volume will expand as shown by Griss et al [26]. This could be used to either drive the flow of a microchannel with a one shot pump, or to completely stop

the flow of a microchannel by expanding and blocking the flow of the liquid. This setup needs a way to heat up the microspheres to $\sim 70^{\circ}\text{C}$ which could be harmful to certain biological reagents.

Another method of active fluid control using heaters is thermo-pneumatic microvalves [27, 28]. A two chamber thermo-pneumatic valve was presented by Takao et al [29]. If the heater that is attached to this valve is turned on, the pressure in the left chamber will increase. This will help to close the gap that is next to the PDMS diaphragm which controls the fluid movement.

By taking advantage of the CCD imager used for detection in the system, the disadvantages of using bulky and expensive equipment are minimized, which will allow for active controls to be used.

2.1.3 CCD Imagers

There are two main types of imagers that can be used in fluorescent detection, Complementary metal-oxide-semiconductors (CMOS) and CCD imagers. These sensors have red, green, and blue filters over different physical cups called pixels. The arrangement of these pixels is known as the Bayer pattern. These filters allow the different wavelengths of light into the appropriate pixel. Once the light has entered the pixel, it is converted to an analog signal. The conversion to a digital signal is where the main difference between CMOS and CCD imagers occurs. In a CMOS imager, this conversion takes place at each pixel, while in a CCD imager, the signal is transported off the chip and uses an analog to digital converter (ADC) to return the digital signal. The values that can be returned are 0-255 (2^8) for an 8-bit binary digit (bit) system. The benefits of using CMOS imagers are low power consumption and price, but the

images taken are generally noisier. A CCD imager offers better image quality and sensitivity at low light, however CCDs require greater power consumption [30].

The unprocessed signal that is returned is the raw data [31]. Typically, for most commercial applications, this data has to go through various smoothing and interpolation algorithms that will fill in the missing pixels so every pixel on every layer has a value. The image is then compressed to a Joint Photographic Experts Group (JPEG) or kept uncompressed as a Tagged Image File Format (TIFF) file. Using raw data will bypass the smoothing and compression steps and give the true value of the data that is seen by the CCD imager.

A benefit of using a lens-less CCD imager is the elimination of the expensive lenses that lead to an increase in the overall cost of a unit and test. Various groups have tried to incorporate lens-less detection into microfluidics. Some of the research performed includes cell counting [32- 35] and use of a CCD as fluorometer [36, 37, 38].

The spectral sensitivity of the raw Fire-I CCD is shown in Figure 1. This figure shows the CCD has a greatest response for green light. It also shows at a wavelength of 607nm, which is the wavelength of emission of the quantum dots used for detection, the red pixels will capture the most light while the green pixels will capture some of the light. The Fire-I CCD is a 1.3 Megapixel camera and takes a 640x480 pixel image.

In order to eliminate some of the noise of the CCD, a calibration image can be taken using Equation (1). The raw image is the actual image taken with the CCD. The dark image is the thermal and dark current error, and is found by taking an image with

no light source and a cap over the lens. The flat field is error over time and is found by taking the dark image over period of time.

$$\text{Calibration Image} = \frac{\text{RAW Image} - \text{Dark Image}}{\text{Flat Field}} \quad (1)$$

Spectral Sensitivity Characteristics (excludes lens characteristics and light source characteristics)

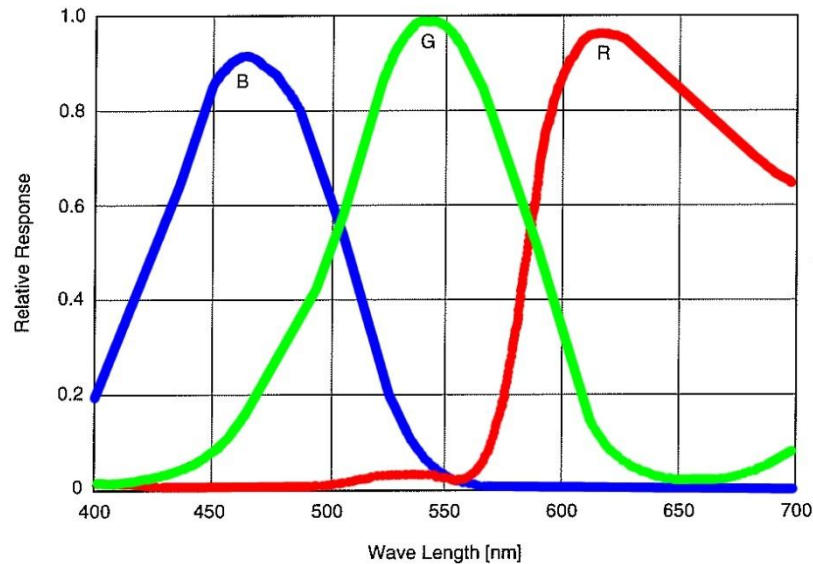


Figure 1: Spectral Sensitivity of FireI CCD
www.unibrain.com/download/pdfs/Fire-i_Board_Cams/ICX098BQ.pdf

2.1.4 Filter Requirements

Optical filters are essential in the use of fluorescent microscopy. There are three main types of optical filters that can be used. These filters are longpass, bandpass, and shortpass filters. A longpass filter, shown in Figure 2, is a filter that will only transmit light that is above a certain wavelength. This figure shows that as the wavelength of light goes up, the amount of light that is transmitted will also increase. Short pass filters, shown in Figure 3, are the same as long pass filters except that they will only transmit light that is below a certain wavelength. The important specifications when selecting either type of these filters are the rejections wavelengths,

and the transmission percentage, which is the amount of the light that is allowed to pass through the filter.

A bandpass filter, which is shown in Figure 4, allows the transmission of light between two distinct wavelengths. A bandpass filter can also be made by combining a short pass and a long pass filter. This type of filter is specified by the center wavelength and the Full Width at Half Maximum (FWHM) or bandwidth value. Another important specification on a filter is the transmittance of light percentage. This shows what percentage of the light that the filter will let through at its center wavelength [39].

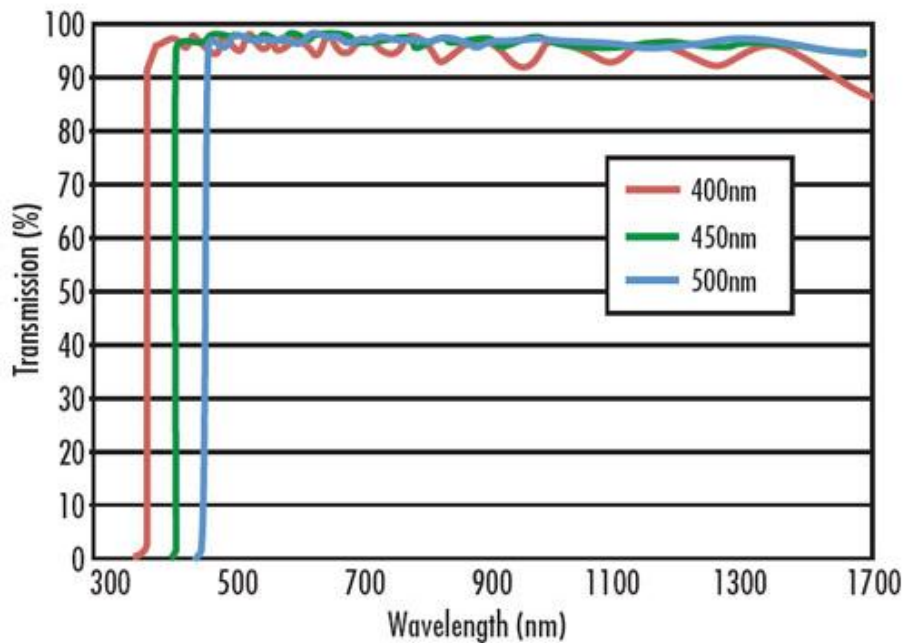


Figure 2: Longpass filter specification from Edmunds Optics
http://www.edmundoptics.com/images/catalog/3044_lineart.jpg

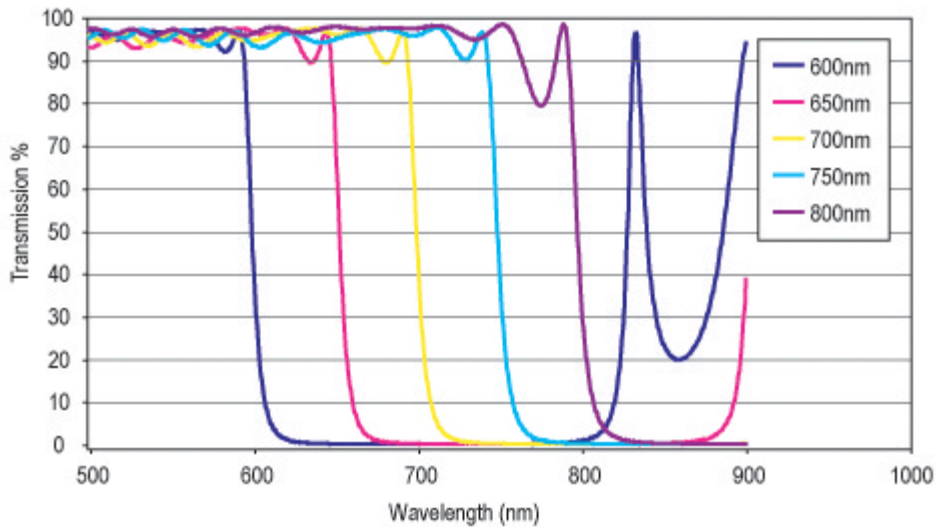


Figure 3: Shortpass Filter
<http://www.edmundoptics.com/images/catalog/7276.gif>

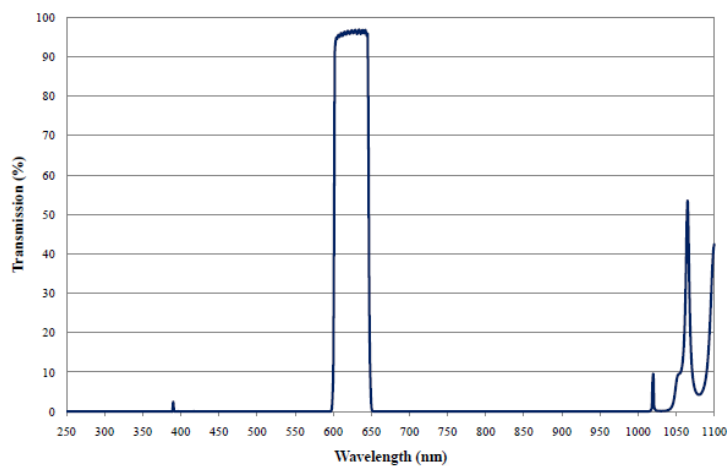


Figure 4: Bandpass filter specifications from Edmunds Optics
http://www.edmundoptics.com/techsupport/resource_center/product_docs/curv_67049.pdf

2.1.5 Biology

The assay protocol that is used in the device for the detection of CRP is shown in Figure 5. This assay is an example of a sandwich protocol and the first step is functionalizing the surface of a PDMS chip with Bovine Serum Albumin (BSA) which allows a layer of Glutaraldehyde to stick to it. The Glutaraldehyde in turn allows for a layer of Protein A to be added. The final step in the functionalization of a chip is the

addition of Rabbit Anti- CRP capture antibodies. These capture antibodies will allow for the binding of CRP from a sample. Once CRP has been captured, biotynalated Goat Anti-CRP detection antibodies can then bind to the CRP. Streptavidin coated quantum dots can then be flown into the detection site and will stick to the biotynalated detection antibodies.

Quantum dots are a type of semiconductor particle that will emit light when excited by a certain wavelength. This characteristic allows for them to be used for fluorescent imaging. Quantum dots are brighter compared to other fluorescent imaging techniques such as fluorescein isothiocyanate (FITC) and phosphor dots. The quantum dots that are used for detection are excited at 405nm and emit light at 607nm.

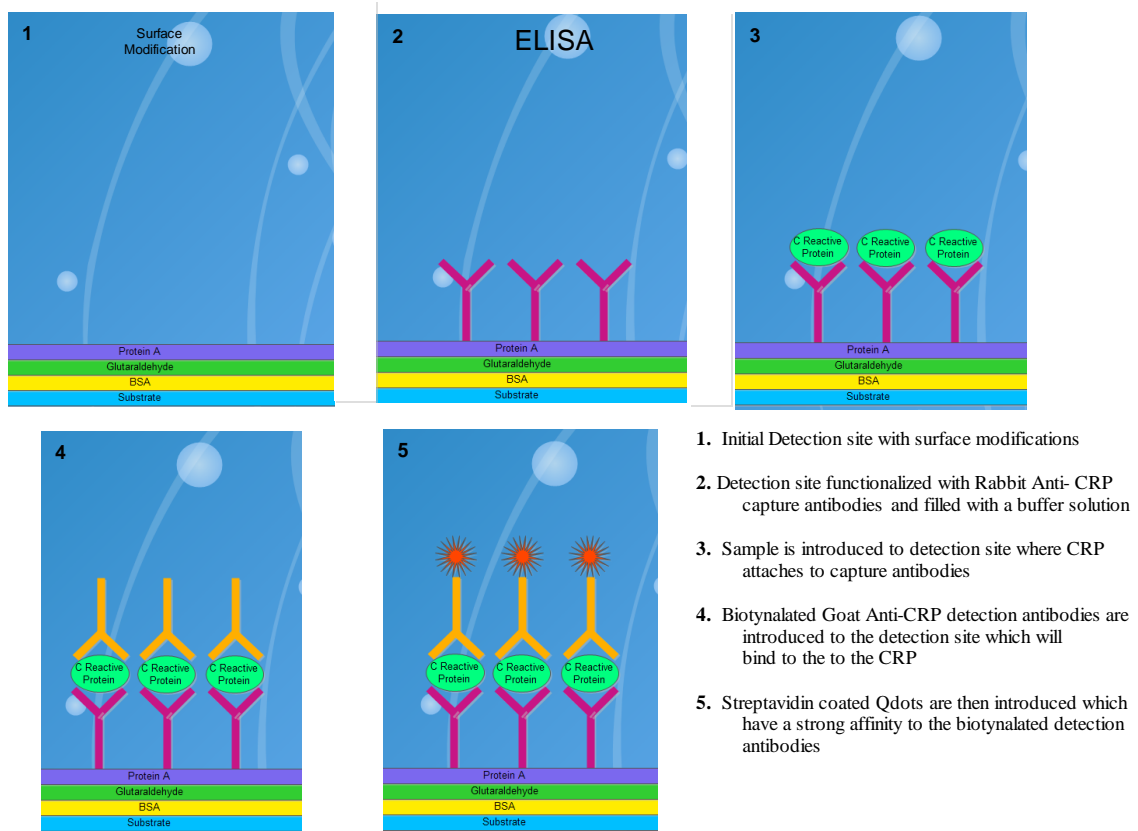


Figure 5. Sandwich assay protocol for detection of C-reactive protein in buffer solution

2.1.6 Edge Detection

Edge detection is an important aspect in image processing because it is a tool that can help to determine important features in an image such as corners and lines. The two most common types of edge detection methods either use a gradient method or a Laplacian method. Figure 6 is taken from the book “Handbook of Image and Video Processing” and shows a continuous function that goes from dark on the bottom to light on top. The middle graph shows the derivative or gradient approach, and the bottom graph shows the second derivative or the Laplacian approach. The gradient approach produces a first derivative in the vertical direction and horizontal direction and determines the point where the function goes from dark to light (x_0) as a local maxima or minima. The Laplacian approach determines x_0 when the second derivative is zero crossing. Gradient methods of edge detection are very good when the gray levels in an image change very rapidly, and Laplacian methods are better when the gray levels change slowly.

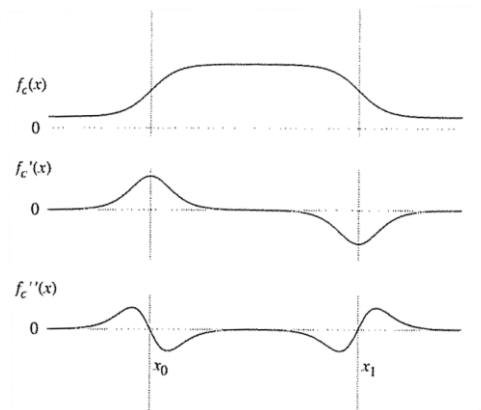


Figure 6: 1D representation of edge detection taken from Handbook of Image and Video Processing p. 536.

The Roberts, Prewitt, and Sobel methods are common methods of edge detection that use a gradient method. An edge detection method that uses the Laplacian method is the Marr Hildreth method.

The Canny method of edge detection [40] combines elements from both the gradient and Laplacian methods. John Canny had three goals when engineering this method. They were to minimize the errors, have good detection of edges, and determine the edges close to where they actually were in the image [41]. According to some papers that have compared various edge detection techniques, the Canny method is the preferred method of edge detection [42, 43].

2.2 Smartphone Integration

2.2.1 Network Background

One of the main ways that information is transferred on the internet is using the 5 step Transmission Client Protocol/ Internet Protocol (TCP/IP). This protocol has multiple layers and specifies how the data should be transferred. The lowest layer that is on the hardware level is the Network Interface layer and deals with how data is physically sent through the network. This uses the Ethernet protocol and usually takes place using various hardware devices. The next layer is the Internet layer which packages the data with source and destination information, and routes the data using IP protocols.

The third layer is the transport layer which is how the data is actually delivered. There are two different protocols used to send data: TCP and User Datagram Protocol (UDP). The TCP protocol requires a handshaking method called a

three-way handshake in order to establish a connection with each of the hosts. After a connection has been established, the data can be sent and received. If data is lost along the way then whatever device is receiving the data can request it again. Before the connection is closed, the three way handshake will occur again to make sure that all of the data has been sent and received. This type of transfer is good for applications where it is important to receive all of the data in the correct order such as sending emails or images [44].

The other type of protocol, UDP does not use a handshaking method and will send the data out regardless if the receiving device is listening or not. The UDP transport protocol is faster because of a smaller header size which can be advantageous in situations where there is a lot of data being sent at a very fast rate; such as video streaming or online multiplayer games.

The final layer is the application layer, which works regardless of UDP or TCP transport protocols, and is how programs can interact with the data. Some common protocols in this layer include Hypertext Transfer Protocol (HTTP), File Transfer Protocol (FTP), and Secure Shell (SSH), as well as many others [45].

An Internet Protocol (IP) address is the location of a device on a network. The two types of IP Address protocols are the 32 bit IPv4 and the newer 128 bit IPv6. The IPv4 protocol can only support 2^{32} (4,294,967,296) addresses, however a large amount of these addresses are reserved and cannot be used by the public. The total amount of IPv4 addresses available to the public are about 2.9 billion. Due to the finite amount of IP addresses, the IPv6 protocol was established and the total amount of IP addresses using this protocol is 2^{128} ($\sim 3.4 \times 10^{28}$) [46].

An IP address can also be either external or internal. An external IP address is the address that is assigned by the Internet Service Provider (ISP) while an internal IP address is what is used in most home or private networks. The external IP address will connect to a router, and the router will split the address into internal IP addresses that are assigned to different devices. This process is shown in Figure 7.

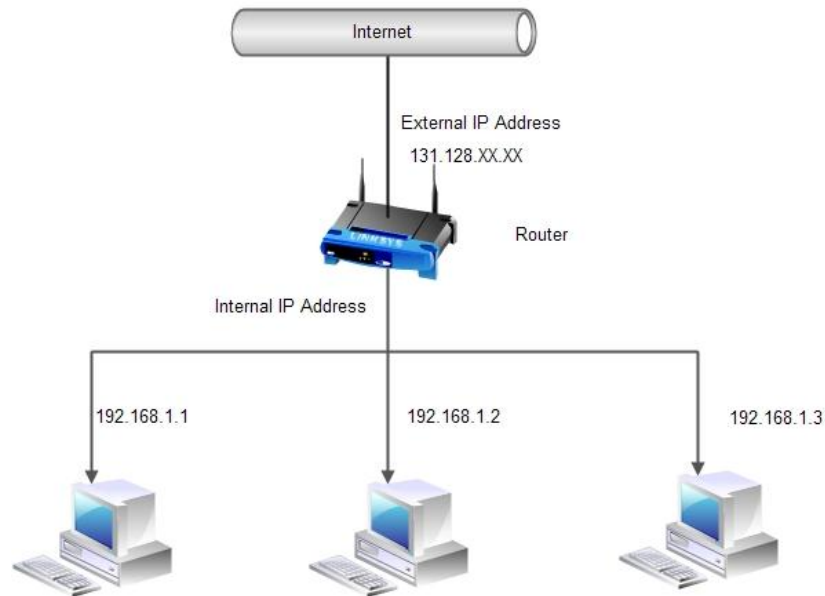


Figure 7: Internal vs. External IP Address

A server client connection scheme shown in Figure 8 requires one device, the server, to be constantly listening for a client to make a connection. Once the client is connected, the server will recognize the connection and perform whatever its next action is (i.e. run a program, send back information). If a client requests data from a server, it is a GET request and if data is submitted, it is a POST request. In order for a client to make a connection to the server, it needs to know the port that the server is listening on.

A port is a 16 bit unsigned integer (0-65535) and is the channel that the data is sent to. The ports 0-1023 are well known ports and are reserved. Some examples

include port 80 which is reserved for HTTP and ports 20 and 21 which are for File Transfer Protocol (FTP). Ports 1024-49151 are the registered ports, and ports 49152-65535 are private ports [47].

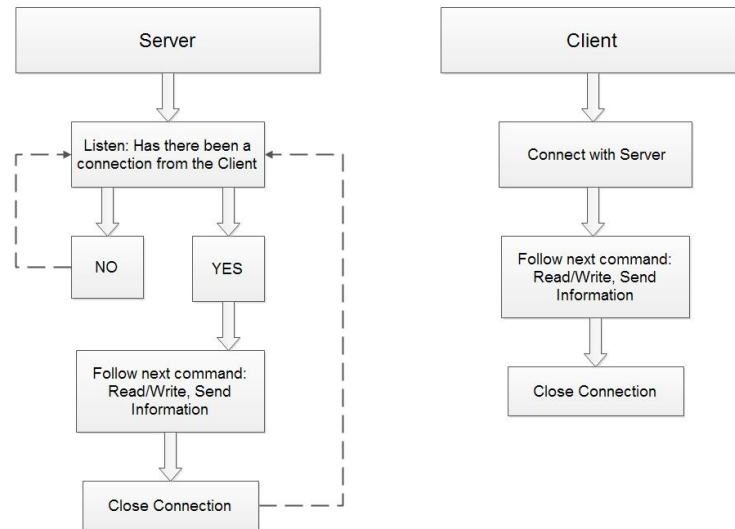


Figure 8: Server Client Representation

2.2.2 Wireless overview in Medical Devices

It has become increasingly apparent that mobile technology has the ability to transform certain aspects of the medical industry. Smartphone apps can be created and used to access patient records [48], check vital signs, and help physicians make better decisions regarding patient care [49, 50]. Apps can also be created for student study guides, clinical consults, and anatomy and drug references [51, 52]. This is particularly true for urologists and surgeons where apps have been created that allow them to view radiology images, keep a surgical logbook, and communicate with other specialists in their respective fields [53, 54, 55].

There have been recent technological advances that have incorporated wireless technology into medical equipment. These wireless devices have been used to monitor

the tremors of patients with Parkinson's disease [56, 57], monitor electrocardiogram (EKG) data from a patient [58, 59, 60], monitor vital signs and track patients during an emergency [61, 62, 63], as well as monitor patients with nasal obstruction and send results to a smartphone [64].

Additional devices with wireless integration include the Cadi ThermoSENSOR thermometer that continuously measures body temperature and sends the data to a computer [65]. This device is an improvement over a thermometer that used an iButton for recording data, but had to be connected to a computer in order to retrieve the data [66].

Wang et al [67] has shown that a smartphone can be used for an automated mobile application. This test uses an Enzyme-linked immunosorbent assay (ELISA) to detect the presence of Human epididymis protein 4 (HE4) from urine. A urine sample is loaded onto a chip where a colorimetric reaction would occur when a substrate was added. The intensity of color would indicate the amount of HE4 in the urine. Then an image would be taken with a camera and using a mobile app, the HE4 concentration could be instantly determined.

Implantable systems are also starting to become prevalent. Systems such as the artificial retina [68] aim to incorporate wireless capabilities to send information to and from the device. Another implantable device, a pacemaker, by Home Monitoring (HM) provides the capability to upload the stored data from the pacemaker to a secure website [69].

The National Aeronautics and Space Administration (NASA) have awarded grants to various companies that are trying to create tests that incorporate smartphones

for blood-based diagnostics. One of these grants proposes the use of a modified smartphone because of its high resolution camera to detect different biomarkers within a clinical range, which will be analyzed on a computer [70]. Another NASA grant proposes the use of wireless optode sensors for fluorescence signal detection and for the data collected from these sensors to be delivered to a smartphone to be analyzed [71]. These systems will give NASA the ability to self-monitor certain conditions of crew members during different missions.

2.2.3 Competing Point of Care Devices

A few portable and handheld POC devices have recently been designed however the majority of these devices do not contain integrated wireless communication. The device either has to be connected to a dock, or to a computer in order to upload and send the results. Some of these handheld and portable devices include the APOCIS by the University of Rhode Island [72], the Triage Cardiac Panel by Biosite [73], the i-STAT and i-STAT1 Wireless by Abbott Point of Care[74], the Banalyst by ROHM [75], the Handheld Flow Cytometer By Diagnostic Chip (DC) LLC [76], and a handheld detection system that analyzes foodborne pathogens by the University of Arizona [77].

APOCIS is a portable POC device that was developed by Faghri and Li [72]. The device is the size of the shoe box and can be used for the detection of CRP. This device uses a fluorometer and needs to be hooked up to a computer for analysis and to deliver the results which can be obtained in 15-20 minutes.

The Triage Cardiac Panel is a portable battery operated fluorometer that produces a digital readout and printout of the results in approximately 15 minutes.

This device also requires the connection to a computer so the results can be directly uploaded to a laboratory information system [73].

Abbott Point of Care has created a few handheld POC devices, the i-STAT and the i-STAT 1 wireless, which use disposable test cartridges and can run many different clinical tests. However, these tests do not include a test for CRP and are more suitable for different cardiac markers, blood gases, chemistries, electrolytes, coagulation and hematology. To upload the test results, the i-STAT needs to be docked to a downloader, while the i-STAT wireless can deliver results to the patient's electronic record [74].

The Banalyst created by ROHM, uses a drop of whole blood and a chip that can be discarded at the end of the test. The readout of the test is given on the actual device which is approximately 1 foot long, 1 foot wide, and weighs about 20 pounds. The Banalyst has preloaded chips that can test for Glycated hemoglobin (HBA1c), CRP, and high sensitivity CRP (hsCRP)[75].

The handheld detection system designed by You et al [77] is a microfluidic device that is capable of detecting pathogens in fresh produce samples. This handheld battery powered unit is 12.2cm x20.8cm x 5.2cm and is controlled by a microcontroller. The sample is placed in a microfluidic chip which is inserted into the unit and the output from this device is displayed on an LCD screen on the front of the unit.

Reviewing the previous devices that have been developed, and noting the increase of wireless sensors and smartphone integration in various medical applications, it is evident there is a need for a POC handheld system with integrated

wireless capabilities that will give quick and accurate results. A handheld device controlled by a smartphone that will perform a test for CRP and send results back to a smartphone wirelessly does not currently exist.

CHAPTER 3 - METHODOLOGY

3.1 Fluid Handling

3.1.1 Determination of Bayer Pattern

Determining the bayer pattern of the raw Fire-I CCD imager was a crucial step, since the detection aspect of this device will exclusively use red pixels since the quantum dots used emit light at 607nm which is in the red spectrum, and the fluid control for this system exclusively use green pixels. The fluid control needs to use the green pixels because of the combination of the white LED that illuminates the detection site and bandpass filter that is used for the detection of quantum dots. The CCD spectral sensitivity chart (Figure 1) shows that the green pixels will have a response to wavelengths up to about 630 nm. To determine the Bayer pattern, a smartphone app for the iPhone called Color Flashlight was used. This app allowed for the phone's screen to change to different colors (green, red, and blue). The phone's screen was used to illuminate the Fire-I CCD imager for different colors in order to determine the CCD's specific Bayer pattern.

In Table 1, the app Color flashlight was turned blue and when it was shone over the CCD, the blue photosites of the CCD would allow the most light in and have the highest numbers allowing the locations of the blue pixels of the CCD to be determined. The same method was used when the screen was changed to red in order to determine the location of the red pixels, shown in Table 2, and when the screen was changed to green to discover green pixels, shown in Table 3. The Bayer pattern of the Fire-I CCD imager is BGGR and is shown in Figure 9.

253	162	253	162	253	161	253	160	253	162
170	68	172	70	170	70	169	69	169	72
253	162	253	164	253	167	253	163	253	159
170	68	170	75	173	70	170	71	171	72
253	162	253	164	253	166	253	164	253	161
172	75	175	73	171	70	171	73	170	73
253	163	253	165	253	165	253	163	253	163
173	69	169	74	169	70	172	78	169	74
253	166	253	164	253	164	253	164	253	164
174	66	173	75	172	75	174	74	173	72

Table 1: Blue Pixels

76	151	74	153	75	155	75	154	76	155
143	253	143	253	145	253	145	253	147	253
79	152	79	153	75	157	78	157	81	155
142	253	142	253	149	253	146	253	144	253
82	153	80	155	83	159	81	157	82	158
142	253	146	253	144	253	146	253	147	253
76	153	81	153	84	156	81	156	81	160
142	253	145	253	144	253	147	253	148	253
79	152	80	156	82	159	81	157	86	157
146	253	145	253	146	253	146	253	147	253

Table 2: Red Pixels

149	213	149	214	147	212	153	214	147	214
214	135	216	136	214	137	214	136	216	136
152	215	148	215	156	216	149	214	147	213
216	135	217	140	219	136	216	138	216	137
151	214	152	214	155	214	155	216	148	215
214	139	216	135	215	141	215	143	214	133
153	215	151	214	151	214	157	216	153	215
216	138	216	139	216	139	216	140	215	142
156	214	157	215	155	216	151	217	152	214
215	138	216	139	216	142	216	139	216	140

Table 3: Green Pixels

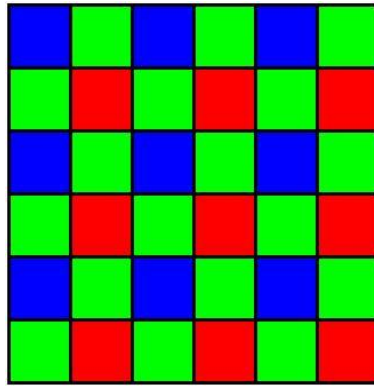


Figure 9: Bayer Pattern of CCD Imager

<http://scien.stanford.edu/pages/labsite/2007/psych221/projects/07/demosaicing/introduction.htm>

3.1.2 Initial Fluid Handling Setup

The initial fluid handling setup was combined with the detection setup. This setup is shown below in Figure 10, and was originally designed just for the detection aspect of this project. Since the detection aspect only uses a Light amplification by stimulated emission of radiation (LASER) diode that is placed at a 90° angle from the CCD imager, there was no need for a light above the detection zone. Using this setup, the cool white LED used for the pumping had to be manually positioned each time since there was no housing that would protect it in order for the CCD to produce an acceptable image.

The microcontroller in this setup was able to turn on and off the cool white LED, the pump, and the LASER diode. This setup used a PDMS chip that was bonded to a piece of glass. The glass was able to slide into the top part of the setup that housed the ultraviolet (UV) LASER diode located above the CCD imager. A close up view of how the glass was able to slide into the setup is shown in Figure 11 This allowed chip to be positioned close to the same spot, relative to the CCD. The CCD was positioned underneath the chip with an optical filter and was also connected to a computer

running MATLAB for image acquisition. An Arduino microcontroller was a practical choice for this application since it can be controlled from MATLAB via a serial input. Arduino microcontrollers can also be programmed to accept commands through MATLAB wirelessly by using the WiShield 2.0.

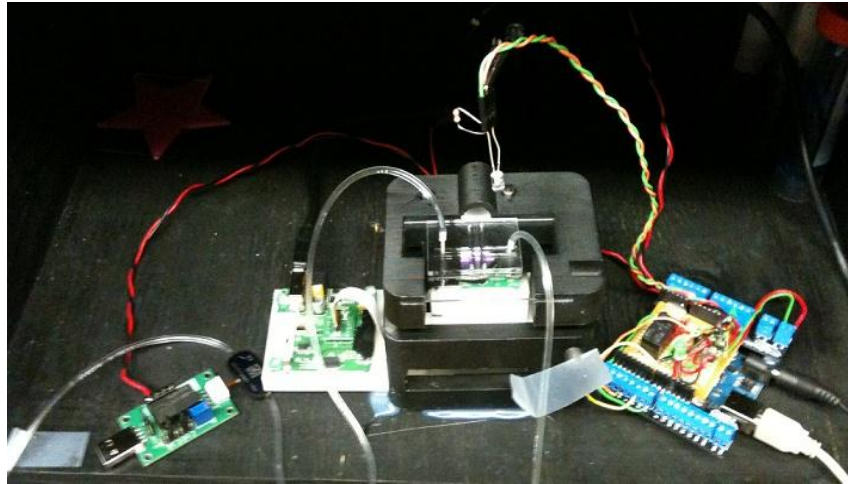


Figure 10: Optical Detection Setup

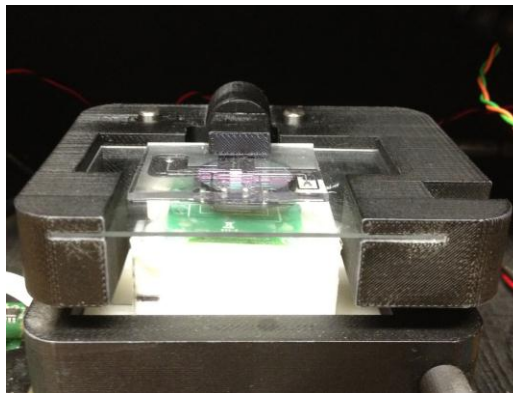


Figure 11: Close up view showing glass slide inserted into stage

3.1.3 Final Fluid Handling Setup

After using the initial setup to prove the concept of feedback control and edge detection, it became necessary to create a new setup that would mimic the final

product's setup. Even though this setup simulated the final product, this setup was solely used for fluid and did not consist of any placement for the UV LASER diode.

This setup used a double layered PDMS chip, similar to those used in the actual test for CRP. Rather than sliding the chip into position like the initial setup did, the chip would be placed over pieces of polyetheretherketone (PEEK) tubing and pressed down allowing for a consistent placement. This setup consisted of an Arduino microcontroller , a Bartels micropump to pump the liquid, a white LED for pumping, orifices to slow down the flow rate of the liquid, a Fire-I raw CCD to obtain the images, and a 607 bandpass filter show in Figure 4. The CCD, like the previous setup, was also connected to a computer running MATLAB for image acquisition and image processing.

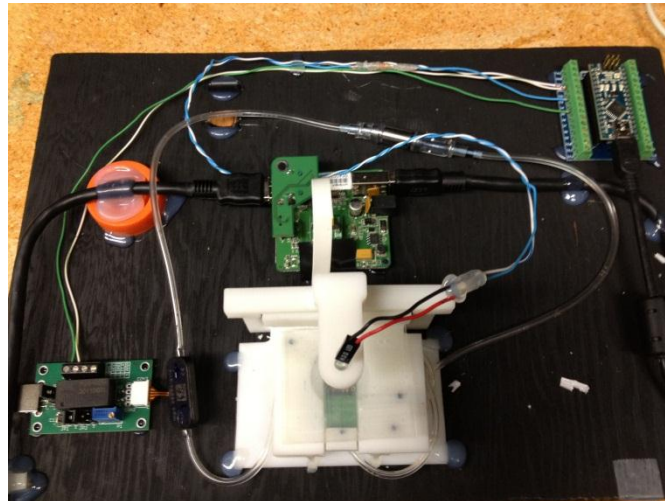


Figure 12: Final Setup for fluid control

A sequentially loaded PDMS chip is shown in Figure 13 with colored water used to represent the various reagents that would be involved in a test. Yellow water represents the sample, blue water represents the washing buffer, red water represents

the labeled detection antibody, purple water represents the reference fluid, green water represents the capture antibody, and black water represents black ink in the waveguide to funnel the excitation light

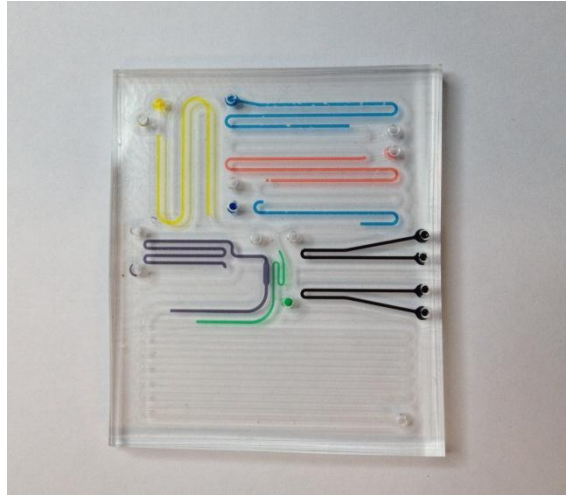


Figure 13: Sequentially Loaded Chip

3.1.4 Change of Design of Microfluidic Chip

The original design of the microfluidic chip had an ellipse as a detection chamber and did not have a calibration chamber. If positioned correctly, this detection chamber would almost take up the CCD's entire frame. An image of this chip's design is shown in Figure 14.

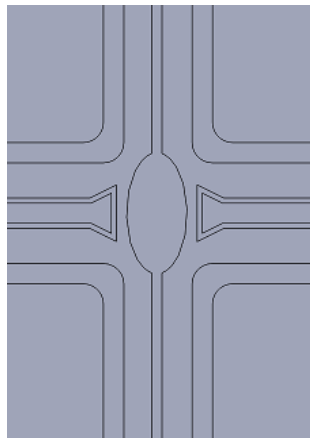


Figure 14: Original Elliptical Chip

Initially, the region of interest (ROI) for the pumping was manually placed directly in the detection chamber. This ROI in the elliptical detection site is shown in Figure 15. In Figure 16, the difference between air and liquid in the elliptical detection chamber is shown. Air is present Figure 16a, and the detection chamber has a darker color overall. Liquid is shown in Figure 16b and the detection site is lighter and has a more uniform color. By taking advantage of these differences, it is possible to create a feedback controller that would look for a change in pixel value in the ROI and determine if there was liquid or air present.

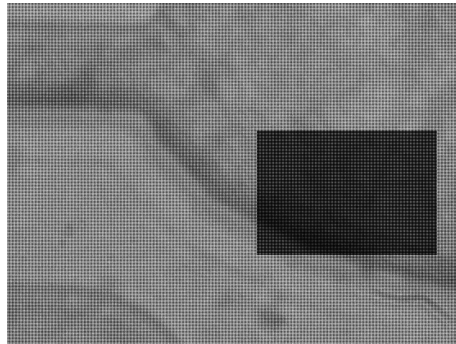


Figure 15: Region of interest placed in the elliptical detection chamber

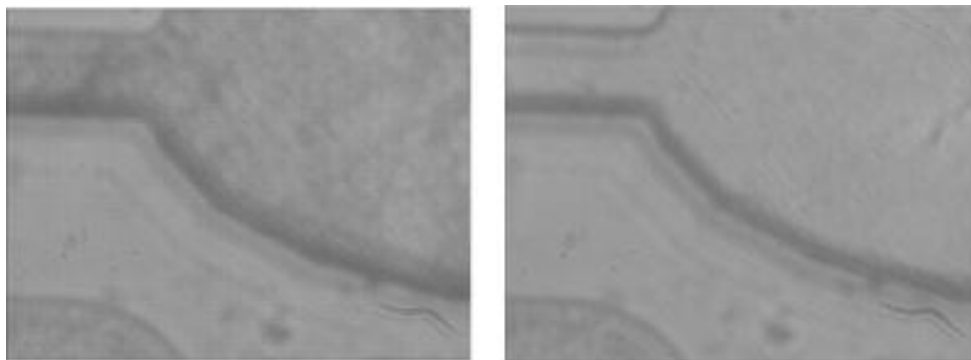


Figure 16: Image of elliptical detection chamber with a) air and with b) liquid

A few different issues arose by using the elliptical detection chamber. First, when pumping liquid many bubbles and air gaps would appear. Another issue that arose was that the detection system needed a way to calibrate itself before every test because the CCD does not always give the same reading on the same concentrations over different days.

To solve the issue with the bubbles, a new 'S' channel was created for the detection chamber. This new 'S' channel design is shown in Figure 17. The 'S' channel allowed for the channels dimensions to stay at a uniform size throughout the entire chip. Another benefit of the 'S' channel was that it increased the surface area that the antibodies can stick to, thereby increasing the sensitivity of the test. The calibration chamber and 'S' channels with air are shown in Figure 18a while the same channels with liquid are shown in Figure 18b. Again, these two images of the 'S' channels and calibration chamber follow the same logic that air makes the channels darker and liquid makes the channels lighter. Figure 19 also shows this difference, as well as showing a 3D histogram of the pixel values of the image. Looking at the 3D histogram, it is possible to see that the vertical height of the pixels when air is in the chambers is lower than when liquid is in the chambers. This also proves it would be possible to look for a difference when there is liquid in the channel versus when there is air in the channel.

The calibration chamber allows for two known quantities of quantum dots at two different concentrations to pass through the chamber where a reading is taken. This reading allows for a detection curve to be set up based on how the CCD imager in the system is responding that day.

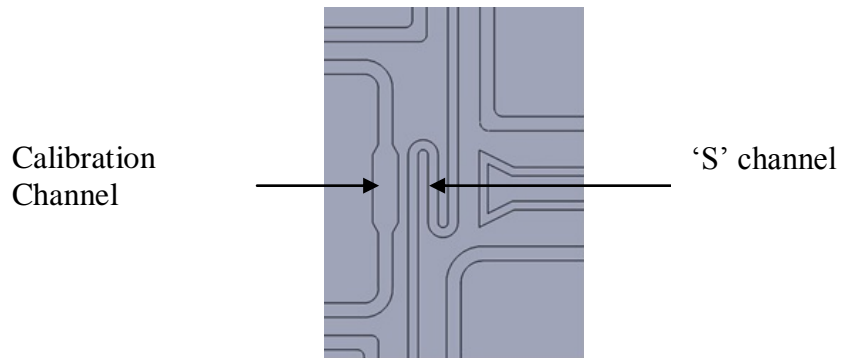


Figure 17: New 'S' Channel design

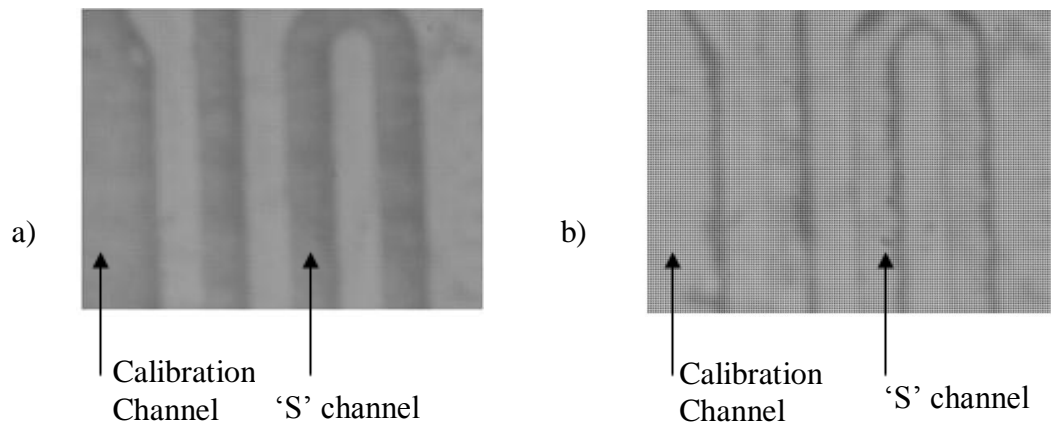


Figure 18: Image of Calibration and 'S' channel detection chamber a) with air and b) with liquid

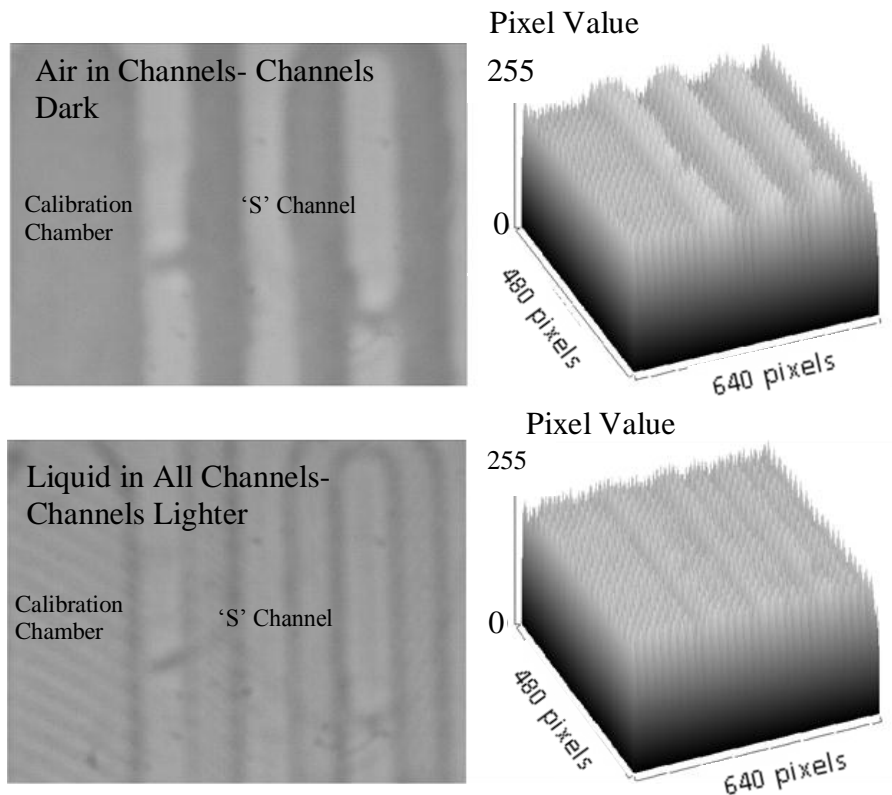


Figure 19: Channels with air in liquid in the detection site along with a 3d histogram on the image

3.1.5 Edge Detection Methodology

Due to small variations with the fabrication of the PDMS chip, even with ports for alignment, the channels are not in the exact same place every time. These small variations in alignment create some error if the ROIs are manually placed with a disregard for the actual image. To try to minimize this error, the control image is first analyzed to determine where the channel ends and the channel wall begins.

Multiple built in edge detection methods found in MATLAB's image processing toolbox were used to try to determine where the different walls in the channel were located. The built in edge detection methods used were Sobel, Prewitt, Roberts, Log, Zerocross, and Canny.

The CCD imager that is used to acquire these images uses the raw data format. This data format combined with the filter and LED used makes certain pixels in an

image unusable. These pixels become unusable with the filter used for detection because the filter will only allow light over 607nm to pass through. This makes the green pixels the only usable pixels since the blue pixels are dark (close to 0) and the red pixels are flooded with light (close to 255). The values of the pixels with this 607 bandpass filter is shown in Figure 20.



Figure 20: Raw data of image; Black are blue pixels, Gray are Green Pixels, White are Red

The image that is taken has to go through an initial modification that will discard the red and blue pixel values. First, the MATLAB function `imadjust` is used in order to spread the intensity of the pixels values to cover the full range of the histogram from 0 to 255. Since the positions of the red and blue pixels are known, their values can be changed to zero using a simple algorithm in MATLAB. Any green pixels with a value of zero are changed to one which ensures none of the green pixels are accidentally discarded if they happened to contain a zero value. Next, any pixel with a value of zero is removed and the image is reconstructed using just the green pixels.

In order to see if it would be possible to detect the channel's edges and to give the greatest contrast of the channels and walls, a chip with no fluid in the detection site was used at first. After the edges were located, an ROI must be placed inside the

channels in order to facilitate the pumping. Different built in MATLAB edge detection functions were used to try to determine the best method for edge detection.

During storage, the PDMS chip will have a TrisEthylenediaminetetraacetic (TE) storage buffer in its channels. Since this buffer is clear, the image will not have as good of a contrast between the channel and the wall. This will increase the difficulty in finding the edges. The same method that was used to determine the edge with air in the detection chamber was used when liquid was in the detection chamber.

A custom method of edge detection that was not a built in method of MATLAB had to be used when liquid was in the channels. This edge detection method would take the average of the next ten pixels in the row, and determine if the current pixel, plus a threshold value, was less than the average value of the pixel. The more pixels that are used to create the average value, increases the ability for the edge detection to find the edges. However, this also increases the distance from the actual edge that the edge is found. By using the next ten pixel values, the distance the edge was found and the ability to find edges was acceptable. This value could be adjusted to fine tune the edge detection.

If the current pixel was less than the average plus the threshold, then the pixel value was turned to white (255) and would mean there may be an edge at that pixel. If the current pixel was greater than the average plus the threshold, then the pixel value was turned to black (0) and nothing of interest was happening at that pixel. The threshold value was found using trial and error and can be changed to make the edge detection more or less sensitive. When the threshold value was too high than the edge

detection becomes less sensitive to small changes and when the threshold value is too low then the edge detection became very sensitive to small changes in the image

After a binary image is created the amount of white pixels in each column are counted. Using the sum function in MATLAB, a white pixel is treated as logically high (1) and a black pixel is treated as logically low (0). A few methods in code are used in order to eliminate false positives detections. These methods make sure there are more than 30 white pixels in a given column, and there are multiple columns of more than 30 pixels next to each other. If a column that is determined to be an edge doesn't meet these criteria then it is discarded and the edge detection moves on to the next column that could work.

After the locations of the channel walls have been identified, the ROI still needs to be placed between the channel walls. Two different methods were used to try to place the ROIs. The first method involved determining the location of every channel and creating ROIs between the channels. The second method took advantage of the fact the channel and channels wall had constant dimensions. After the channel wall of the calibration chamber had been determined, the rest of the channels will be a constant distance from one another. Using this absolute positioning method, finding the edge of the calibration chamber wall becomes the critical step. Each of these methods has advantages and disadvantages. The edge positioning method can give a more accurate ROI since it would fit the channels exactly, however the edge of every channel needs to be accurately found and every false positive has to be eliminated. The absolute method is easier to implement however the ROIs can be slightly off if the edge of the calibration chamber is not found at the same point each time.

After the ROIs are determined, their coordinates have to be transformed back to the original 640x480 image. This transformation has to take into account that in the normal image, the red and blue pixel values are reintroduced. The Bayer pattern of the CCD is shown in Table 4. In the odd columns, the green pixels values occupy the even rows and in the even columns they occupy the odd rows. Knowing that the green pixel locations have both an even and an odd coordinate is important when the ROI is transformed to the complete image.

Row/Column	1	2	3	4
1	B	G	B	G
2	G	R	G	R
3	B	G	B	G
4	G	R	G	R

Table 4: Bayer Pattern

The far right column of the ROI in the calibration chamber will determine whether the ROI needs to be moved over one pixel on the original image. The ROI may need to be moved over one pixel so that the ROI will always begin on a green pixel

The upper left coordinate of the rectangle will always be (10,39) and the height is 360 so the bottom right coordinate is (10,399) making both of these corners fall on a green pixel. If the far right column of the ROI of the calibration chamber is on an odd row then the upper right coordinate will be (Odd,39) and the lower left coordinate will be (Odd,399). These will not be green pixels, so the column the ROI gets lined up with has to be shifted over to the left one so the pixels will become (Even,Odd), shown in Figure 21. For example if the width of the calibration chamber

is determined by the edge detection to be 70 pixels, then the coordinate of the top right corner of the rectangle will be (80,39) and because it is (Even, Odd) it is on a green pixel. Then the length of the channel wall will be about 84 pixels making the left corner of the next ROI start on (164,39) which is still (Even,Odd). However if the width of the calibration chamber is 71 pixels the corner of the rectangle will be (81,39) and will be (Odd,Odd) and be on a blue pixel. Now the width of the wall has to be 83 pixels so the next ROI will also begin on (164,39).

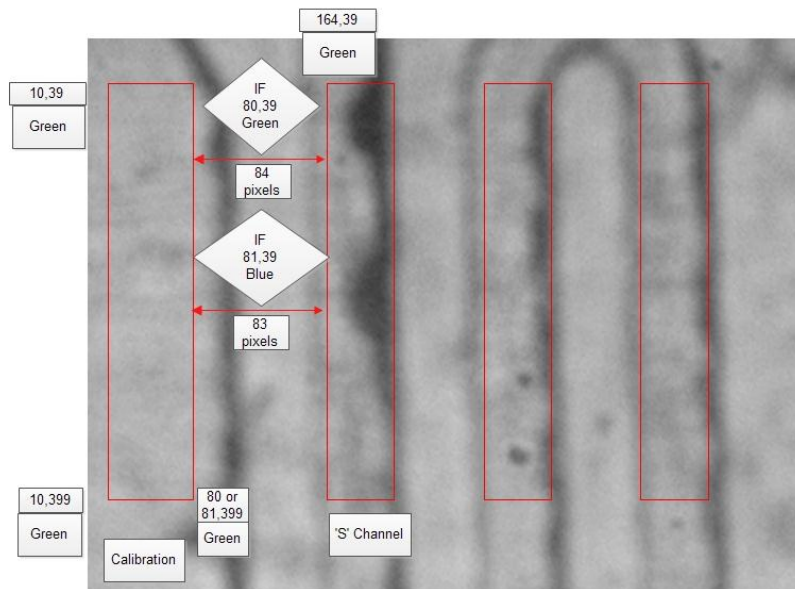


Figure 21: Channel Coordinate Transformation

When this ROI is determined using the method of absolute positioning, it becomes easy to make sure the ROIs of the ‘S’ channel are on the correct coordinates. These coordinates will matter for the feedback pumping so the correct pixels values are being compared. This transformation will not affect the calibration channel’s ROI but will matter for the ROIs in the ‘S’ channels.

Different parameters for the edge detection needed to be determined. First, the color of the LED and the type of filter that would produce the best results needed to be determined. To perform the experiment with the LED and optical filters, the initial setup was used and an Arduino was used to supply the voltage to the LED. Another two parameters that needed to be determined were the height of the LED from the detection chamber and the voltage that the LED runs at. In order to vary the voltage of the LED, a voltage generator was connected to the LED that would allow the voltage to change without varying the position of the chip. A summary of these results and findings as well as pictures from the edge detection methodology will be presented in Chapter 4.

3.1.6 Feedback Control Methodology

The feedback controller that is used for the fluid handling system is an example of an on-off feedback controller. A complete overview of the feedback controller is shown in Figure 22. This chart shows the entire feedback logic that the controller goes through during the course of a sequential loading cycle. At the beginning of the test, a control image with TE buffer in the channel is taken that will be compared throughout the test to determine whether there is liquid or air in the detection chamber.

When the feedback control for the calibration channel or the 'S' channel is started, an image will be taken at a regular time interval and will be compared to the control image by subtracting the two images. A threshold value (normally between 10 to 16) is used and every pixel in the new subtracted matrix is compared to the

threshold value. Typically the feedback controller requires a small amount of noise from the CCD (about 1-2% of the region of interest) for an accurate and sensitive pumping cycle. The noise is the difference that is produced by the Fire-I CCD between two identical successive images when they are subtracted from each other. The threshold value is what changes the sensitivity during a pumping cycle. If this threshold value is too small then the noise of the CCD will typically overpower any change of fluid in the detection site, and the software might think there is a change in the detection site when there is not. If the threshold value is too big then the CCD is not sensitive enough and will not notice when liquid or air goes into the detection site.

If the compared pixel is less than the threshold then the pixel value is set to 255(white) otherwise it is set to 0(black). These pixels are in the format of an uint8 (unsigned integer 8) and can have 2^8 or 256 (0-255) different values.

After the binary mask is created then the white and black pixels are added up. If there are more black pixels than white pixels that means there was a change and there is air in the chamber. However, if there are more white pixels than black pixels, there is still not a change (from the initial state) and so liquid is still in the chamber. After air has been found the program will change from looking to a majority of black pixels to a majority of white pixels.

This control image is also the image that is used for the edge detection and placing the ROI. The first stage of the feedback controller is the pumping of the calibration chamber. The calibration chamber will have known concentrations of quantum dots that will be used to establish the detection curve for that day. First, the pump will be turned on and the program will be looking for air. Once air is detected,

the program will switch to looking for liquid. After liquid has been found, the pump will turn off and allow for the detection to take place. This process will repeat again for the other known quantity of quantum dots and then the pump will look for air for the final time. Once air has been found for the final time then the program will exit the calibration pumping and proceed to pump the 'S' channels.

The pumping in the 'S' channel is a little different because there are three ROI that need to notice a difference instead of just one. Using three ROI were used in order to help with the problem of bubbles that occasionally will occur during a test and to make sure that fluid was completely in the channel.

To try to vary the speed of the fluid, a 4 μ m and a 10 μ m orifice are used. Previous work done in the lab established that a 6 μ m orifice should have been sufficient to slow down the liquid to an acceptable flow rate. However that size was not available to purchase so the next size up and next size down were used. The delay that MATLAB took in between taking different images was varied from 0.5 seconds to 0.2 seconds in an attempt to determine the flow rate of the liquid.

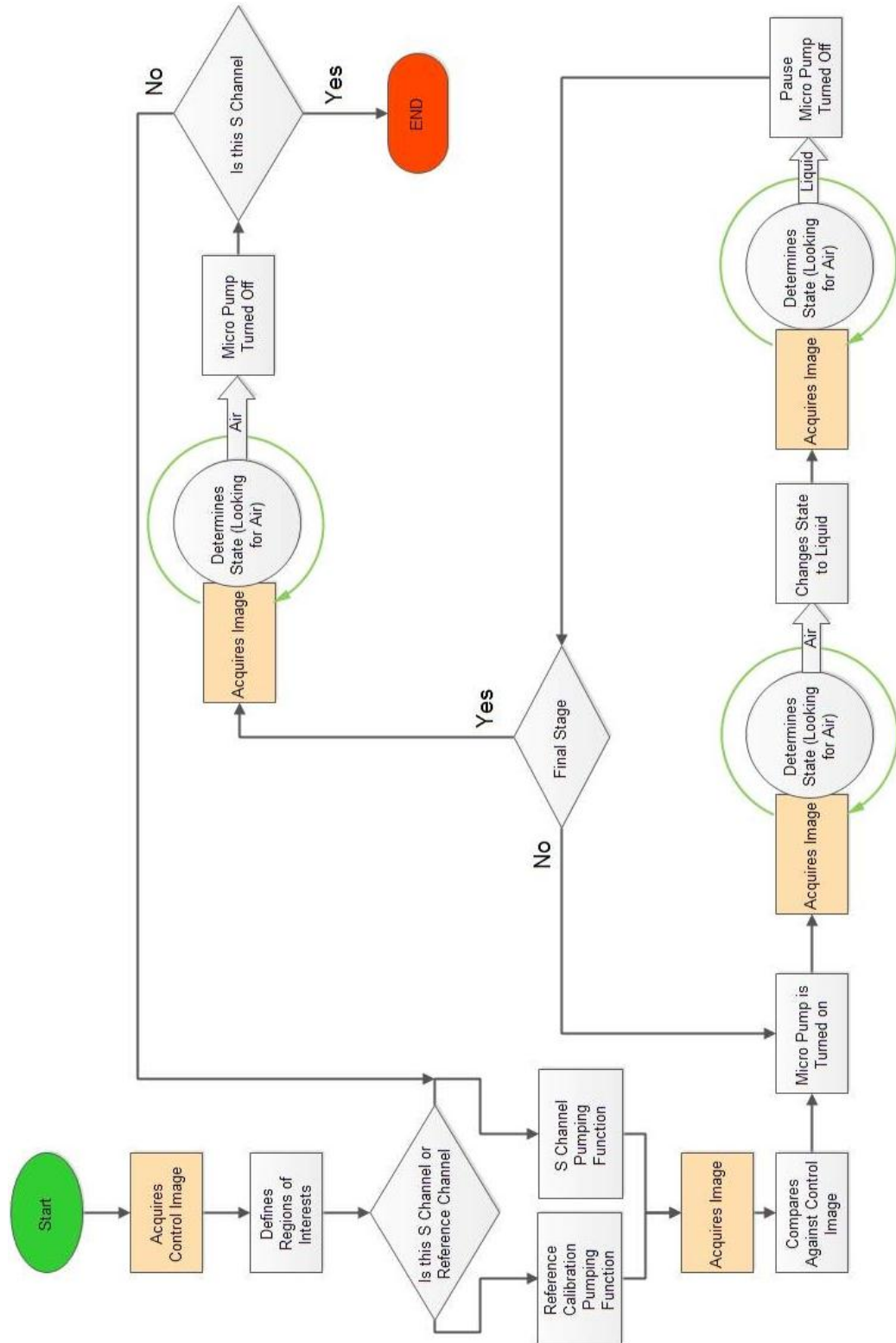


Figure 22: Feedback Controller Logic

3.2 Smartphone and Network Integration

3.2.1 Arduino and Shield

The Arduino was chosen as a microcontroller for this project because of its low cost and open source compiler. Multiple types of Arduino microcontrollers were used for different situations throughout this entire project. The final Arduino microcontroller that was used is a Nano Mega 2560 by Emartee. This microcontroller is shown in Figure 23. To give the microcontroller wireless capabilities, a WiShield needs to be used. The Copperhead WiFi Shield which is designed to work with an Arduino Uno, is shown in Figure 24. This shield is compatible with all of the WiShield 2.0 libraries that are provided by AsyncLabs. Since the Arduino Mega Nano is built by a different company than Arduino, special modifications have to be made so the Wifi Shield will work on the microcontroller. These hardware modifications include remapping the pins of the Wifi Shield so it will connect to the Arduino and software modifications in the WiShield's SPI.H file and the WiServer.h file. The hardware modifications happen because the pin layout of the Mega differs from that of the normal Arduino Uno. On the Nano Mega, the Master In Slave Out (MISO) is pin 50, the Master Out Slave In (MOSI) is pin 51, the Serial Clock (SCK) is pin 52 and the Slave Select (SS) is pin 53. Additionally the System Clock Line (SCL) had to be remapped to pin 21. On the Arduino Uno these pins are 9, 10, 11, 12, and 2 respectively.



Figure 23: Arduino Nano Mega 2560 by Emartee

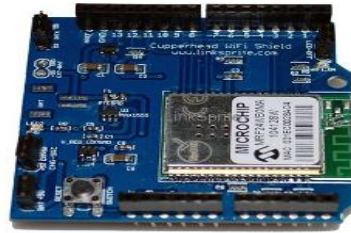


Figure 24: Copperhead Wifi Shield

After the Arduino has wireless capabilities, the Arduino can act as either a server or a client. Normally the Arduino will be acting as a server in order to turn different ports on or off. The Arduino will need to connect to an existing network (such as a home network) and will be given a static IP address (ie. 192.168.1.125). Each port will have a different uniform resource locator (URL) that they will go to. For example, turning a pump on would be 192.168.1.125/pumpon while turning an LED on would be 192.168.1.125/ledon. This could be repeated for as many ports as the user wanted to control. During certain points in a test, the Arduino has to act as a client and send out a GET request to a server.

3.2.2 Environments

Many different developmental environments were used in the creation of software for various parts of this project. A complete list of all of the different programming environments and their purpose are summarized in Table 5. Various Python scripts and libraries were used over the course of the project. One of the most important libraries that was used was the open source Twisted Networking Engine. This engine handled the communication between the iPhone app and Python Server.

Arduino 0022 was the compiler that was used for this project because newer compilers such as Arduino 0023 and Arduino 1.0 had different default libraries and problems with integrating the wireless libraries. All of the code is located on a hard drive in the microfluidic lab at URI.

Environment	What is Controlled
Motodev and Eclipse	Java server used for Android App communication and development of the Android App.
Xcode and Interface Builder	iPhone development software on Mac computer
Python	Server used to get information for the iPhone app as well as various scripts for network performance.
Visual C#	Environment to program the Fast and Easy (FEZ) cobra microcontroller
Arduino 0022	Environment to program the Arduino microcontrollers and various Touchshields

Table 5: List of programming environments

3.2.3 Network

A key aspect to this project is the ability to have a server setup and listening on a remote computer. This server in conjunction with the microcontroller will be able to control the test by running MATLAB after the test has been started by the user. The wireless handheld communication is shown in Figure 25, and shows how different aspects of the test should be able to communicate to one another.

The server will have multiple Python scripts acting as their own servers on different ports and when accessed by a microcontroller they will be able to perform a certain task such as opening MATLAB or receiving and storing a picture.

(1) A user will have control over the test and will be able to start the test with a custom smartphone app and send the patient information to a server.

(2) After the test is started from the smartphone, the microcontroller will receive instructions to begin the test.

(3) At various points during the test, the microcontroller has the ability to connect to the server to facilitate pumping. MATLAB will have the ability to communicate directly with the microcontroller if there is a problem with the test or to tell the microcontroller what to do next. Once the microcontroller finishes its part of the test, it will be able to send a signal to start MATLAB on the server so the analysis of the test can be performed and the results can be obtained.

(4) MATLAB will run a script that will perform analysis on the images obtained during the test. When MATLAB has finished performing the analysis, the results are sent back to an email address as a Portable Document Format (PDF) report and also sent to the smartphone. The information on the PDF report will be generated by MATLAB using the information that was sent from the smartphone app.

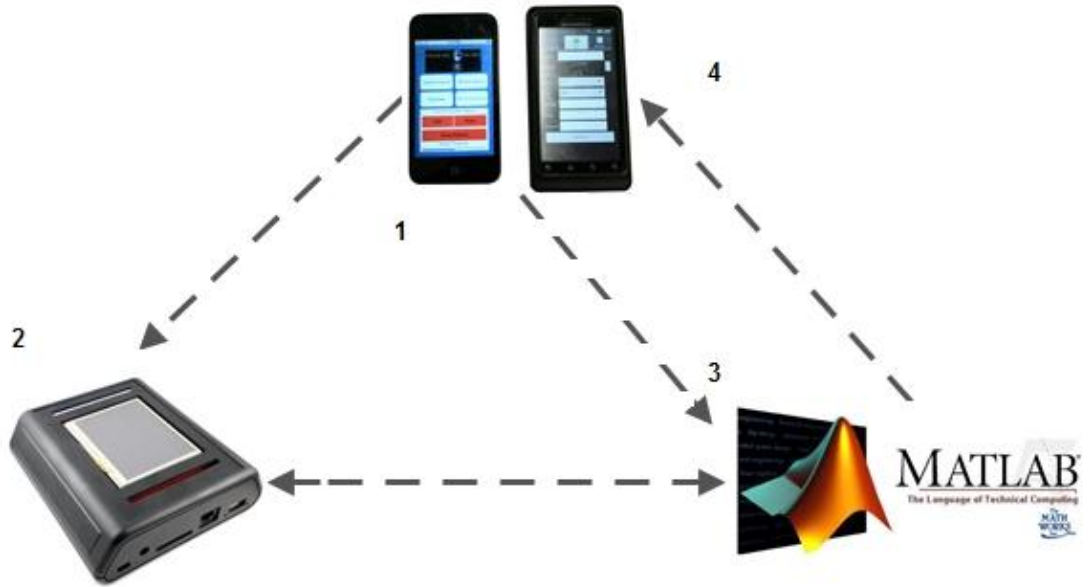


Figure 25: Wireless handheld Communication

CHAPTER 4 – FINDINGS

4.1 Fluid Flow Control

4.1.1 Edge Detection with air in channels

To determine if it was possible to find the edges of a microfluidic channel, edge detection algorithms were originally ran with air in the channels. The air in the channel gives the greatest amount of contrast between the channels and the channel walls. The various methods of edge detection that were built in to MATLAB were used and the results are shown below in Figure 26. The results shown in Figure 26- Figure 32 use the same image for analysis.

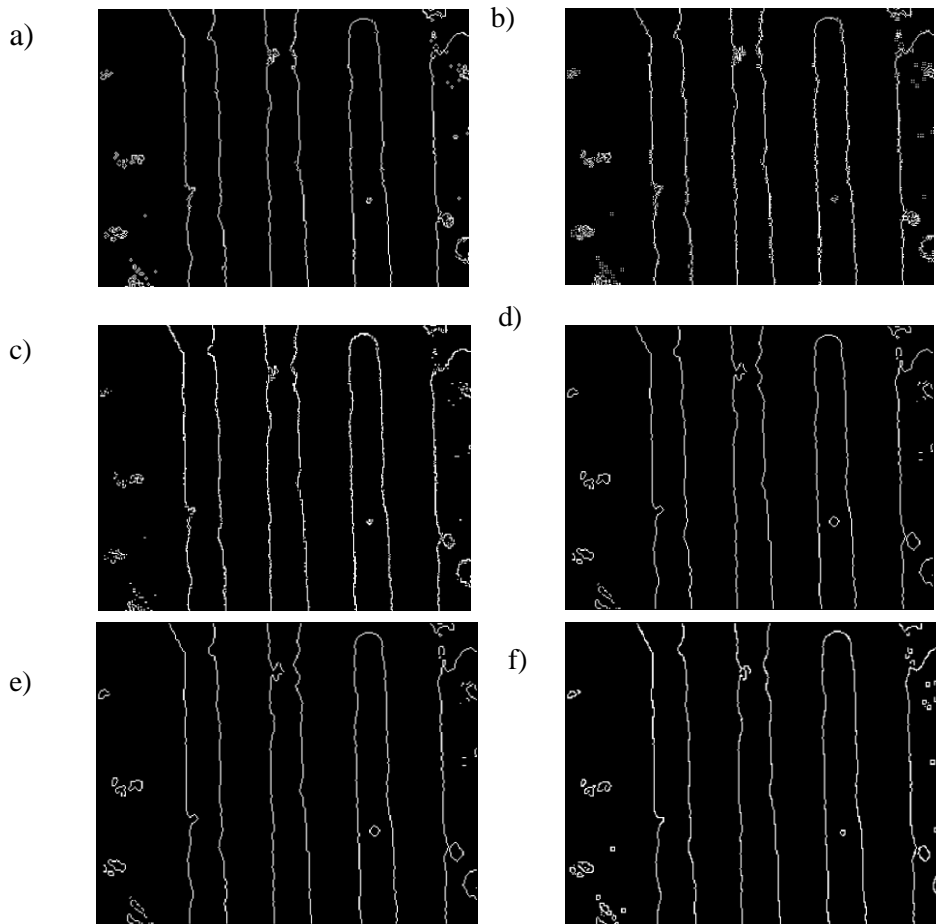


Figure 26: MATLAB Image Detection Methods a) Sobel b) Prewitt c) Roberts d) Log e) Zerocross f) Canny

. When PDMS channels were filled with air, MATLAB was able to detect the edges using all of the different methods. All of these methods produced similar results. Below, Figure 27 was an attempt to place the ROIs in the channels automatically using the built-in edge detection methods with air in the channels. All of the edge detection methods were able to accurately place the ROIs completely in the channel when air was present.

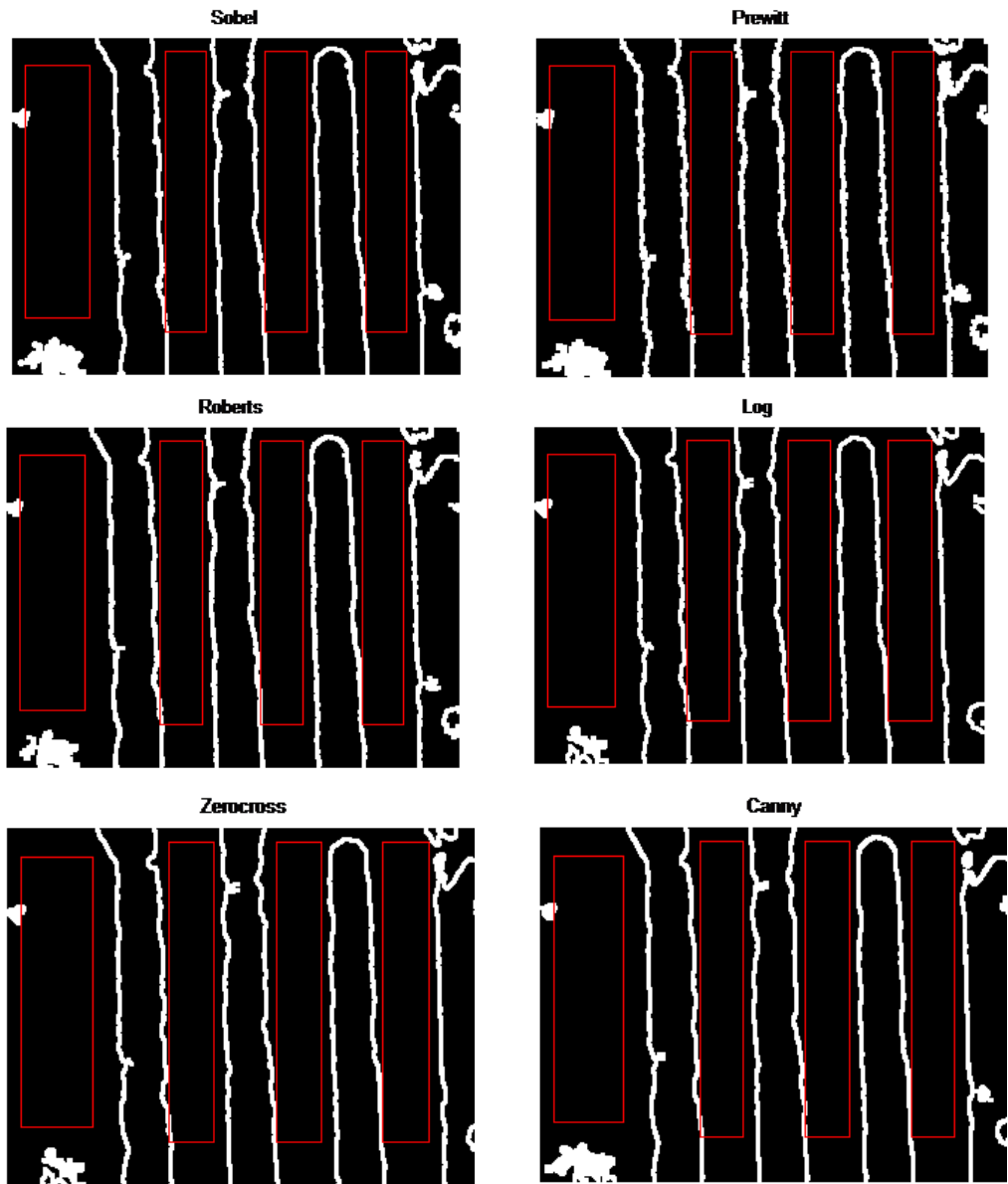


Figure 27: ROI of interest of different edge detection methods with air in channel

Below, in Figure 28, the Sobel method of edge detection was used to determine all of the edges, and place the ROIs inside these channels. These images were taken over a span of multiple days. In contrast with certain aspects of detection, the properties of the CCD do not hinder MATLAB's ability to determine the edges and place the ROIs. The method of placing the ROIs that was used for this test was finding and keeping track of every column that an edge was located at and placing a ROI in between these columns.

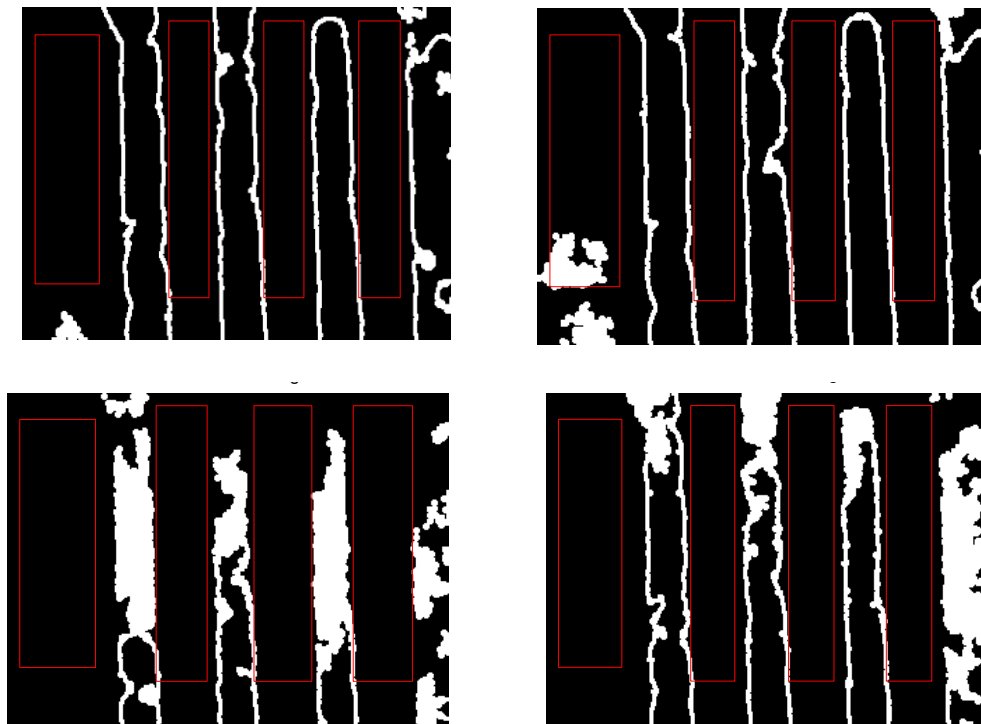


Figure 28: Region of Interest with air in channels over various days

4.1.2 Edge Detection with Liquid in Channels

The results for the edge detection when liquid is placed in the channels are shown in Figure 29. The same procedure from when air was in the detection chamber

was used. The results of using these methods were not good because the ROIs that are placed are all over the place and not always in the channel. The method of placing a ROI was still finding every column that an edge was at and then placing a ROI between the columns. From the images below, the calibration chamber had a lot of false edges inside it so the program would lose track of the numbering of the edges. This is why the second ROI from the left is on a channel wall instead of in the channel.

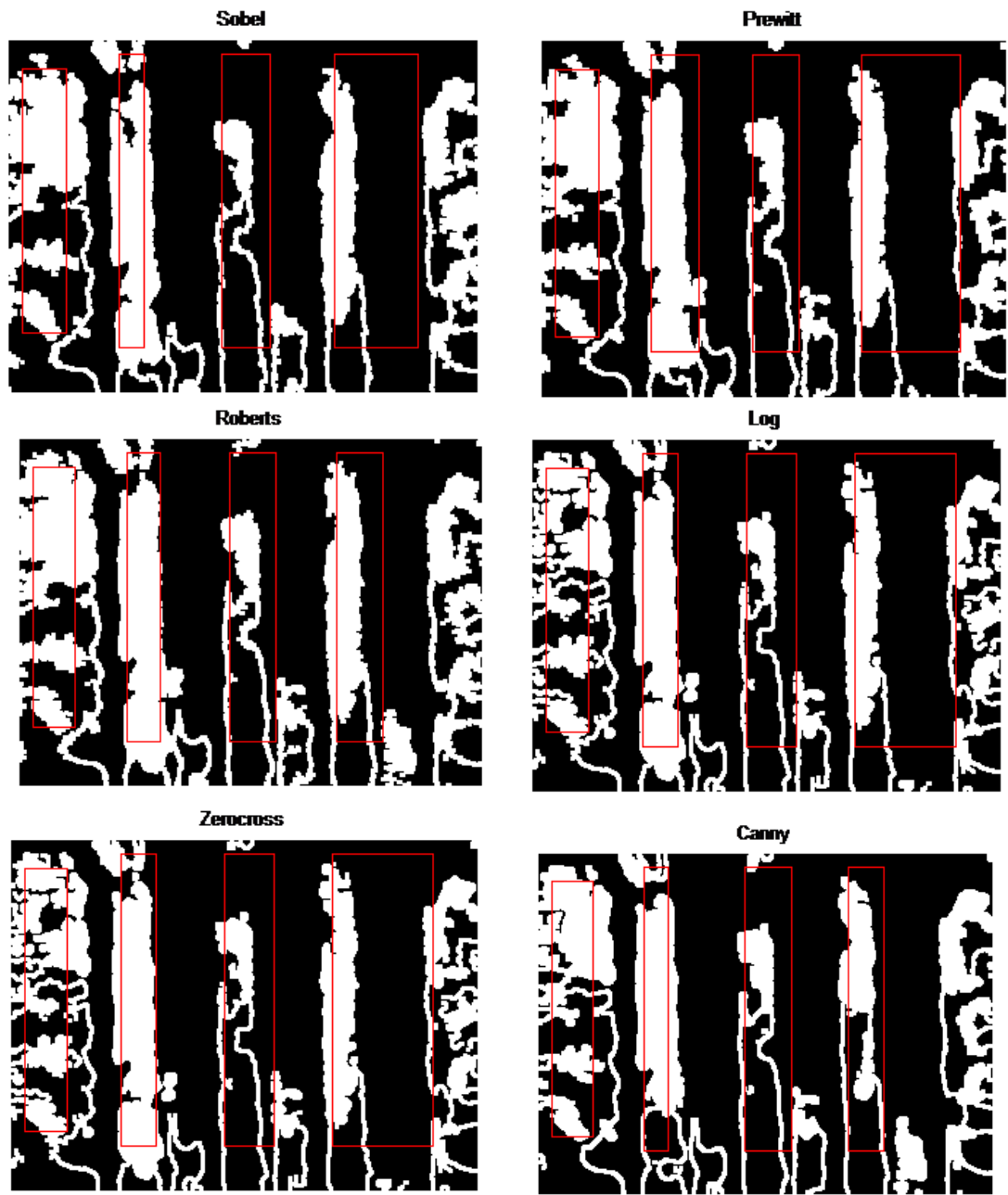


Figure 29: ROI of different edge detection methods with liquid in channel

The same image that was used with air and liquid in the chambers is shown in Figure 30. These results are using the custom edge detection method that was not a built in feature of MATLAB. Using the technique of averaging the next ten pixels, a

fairly accurate representation of the edges can be determined. Figure 30 also shows the image after the ROIs have been placed. The figure below shows the ROI is completely in the calibration chamber and the ‘S’ channels. Overall, this method of edge detection works much better for this project, and allows much more control about what is seen than the built in functions of MATLAB.

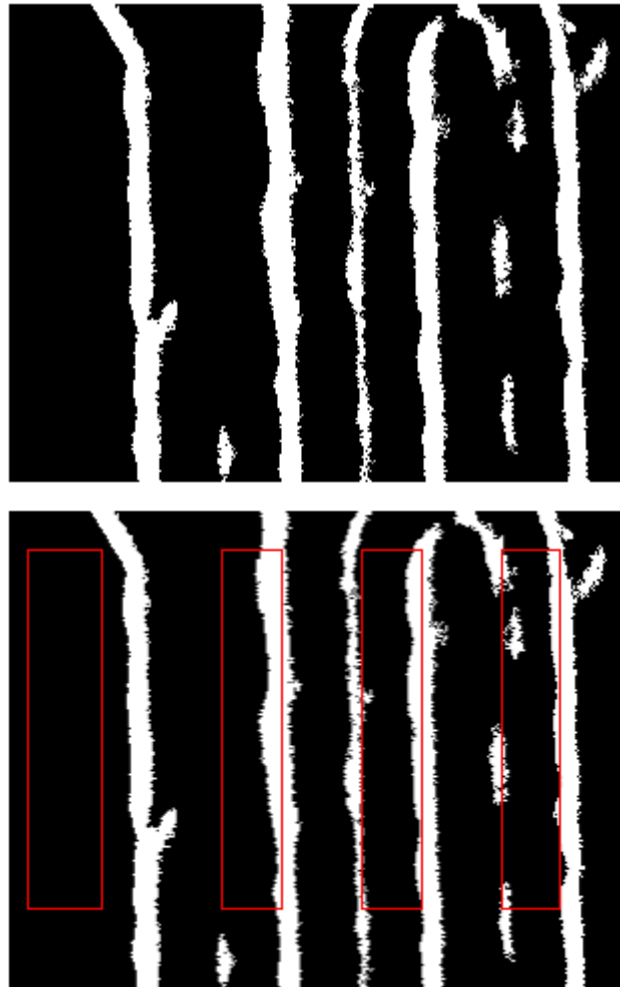


Figure 30: Binary Image with new Edge Detection and Region of Interest

Two different methods of placing the ROIs were used. The first method, the edge positioning method, is shown in Figure 31 and the second method, using absolute

positioning is shown in Figure 32. Overall the method of using absolute positioning works much better than the method of edge positioning since there are less edges that need to be determined. This will decrease the amount of errors that can occur while running the edge detection and the rectangles will always be a fixed width. Using the edge positioning method, it is absolutely imperative that every edge is accurately determined. Figure 31 illustrates what will happen if one of the edges is missed. One of the ROIs in the 'S' channel was not positioned correctly which leaves that entire ROI useless. The algorithm was not able to determine the left edge of the final curve of the 'S' channel but was able to determine the right. This means that the left edge was also determined by the program to be at the right side which created a ROI that is only a few pixels wide.

The absolute positioning fixes this problem since the only edge that really needs to be determined is the edge of the calibration chamber. After this edge is determined the rest of the ROI have a fixed width and the results are shown in Figure 32.

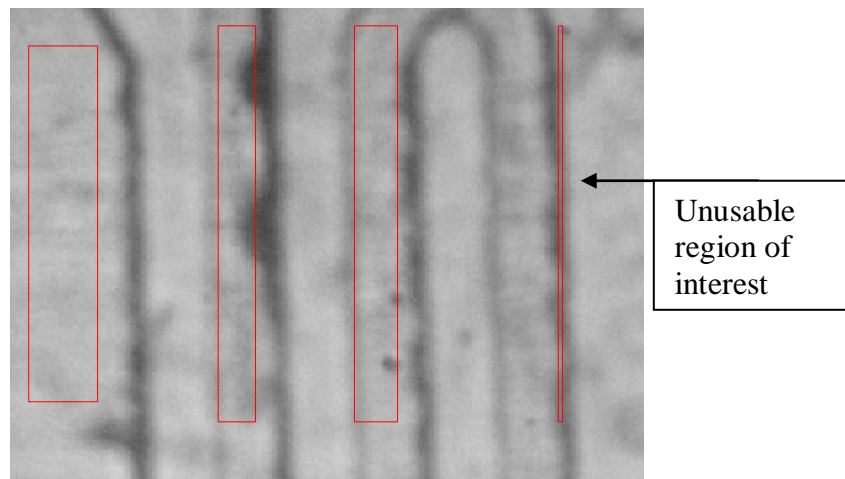


Figure 31: Region of Interest placement finding all edges

Absolute Positioning

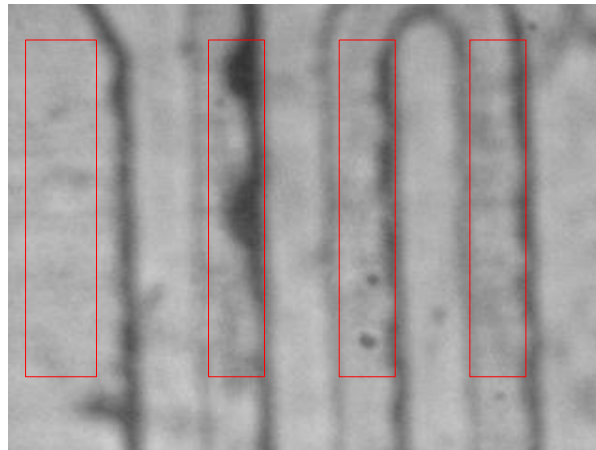


Figure 32: Region of interest Placement using absolute positioning

4.1.3 LED and Filter Parameters

A study was undertaken to determine the best combination of LED's and filters. A list of LED's and their properties are shown in Table 6, while a list of the filters used and their properties are shown in Table 7. Complete listings of the combinations that worked and did not work are shown in Table 8.

In Table 8, a '✓' denotes that the edge detection software was able to accurately place the ROI and the feedback software for pumping was able to determine a difference and stop and start the pump accordingly and an 'X' means it was not.

Color Wavelength(nm)	Manufacturer	Part Number	Viewing Angle (degrees)	Luminous Intensity
Red (643)	Jameco	333973	36	75mcd
Amber Flat (605)	LUMEX	09J9272	110	5mcd
Amber (596)	CREE	02P7166	30	5cd
Cool White (380-750)	VCC	57P7152	100	1.8cd
White (380-750)	VCC	50P9329	30	7cd
Cyan (480)	CREE	04R6672	15	11cd
UV (365)	Cree	67-2133-ND	80	--
Yellow (585)	Vishay	751-1148-ND	28	10mcd

Table 6: List of different LED parameters

Filter	Mfr.	Part Number	Center Wavelength	Rejection Wavelength	Transmittance (%)	Bandwidth
607 bandpass Filter	Edmunds Optics	84102	607	--	93	36
532 10fwhm	Edmunds Optics	65700	532	--	>=45	20
Wratten no 12	Kodak	54467	--	--	--	--
Square bandpass filter	Schott	46054	526	--	--	106
483 bandpass	Edmunds Optics	67028	482.5	--	93	31
500 nm Longpass	Edmunds Optics	47616	--	200-480	>85	--

Table 7: List of different filters and specifications

The cool white LED was the best LED and was able to determine the edges regardless of the filter used. This makes sense because white light is comprised of all wavelengths of the visible spectrum. The other LED that was able to determine the edges of the channel through different filters was the flat amber LED. Both of these LEDs also had a very high viewing angle so their light was not concentrated right at the detection zone, potentially flooding it with light. This happened with the white LED as the viewing angle was only 30° and when shone on the detection site, flooded the CCD imager. The results for the cool white LED are shown in Figure 34. This figure shows that with the cool white LED, it is possible to accurately place the ROI independent of the filter that is used.

The Kodak Wratten Filter that was used had a lot of wrinkles since it was a flexible filter which is why the image produced with that filter is not completely clear. The specifications of the Wratten filter are shown in Figure 33. The images shown in

Figure 34 are not exactly the same since the chip needed to be lifted up and moved in order to change the filter below it. The images from the amber LED that were able to produce acceptable results are shown in Figure 35. The images produced with this LED are generally darker since the amber has a defined wavelength of 605nm which means the filters will cut out more of its light.

Overall, the cool white LED gave the best results. The filter that was chosen was determined by the detection aspect of the system and only the Ultraviolet (UV), Cool white, and Amber LEDs were able to find the edges with the cool white LED producing the best looking and most defined image.

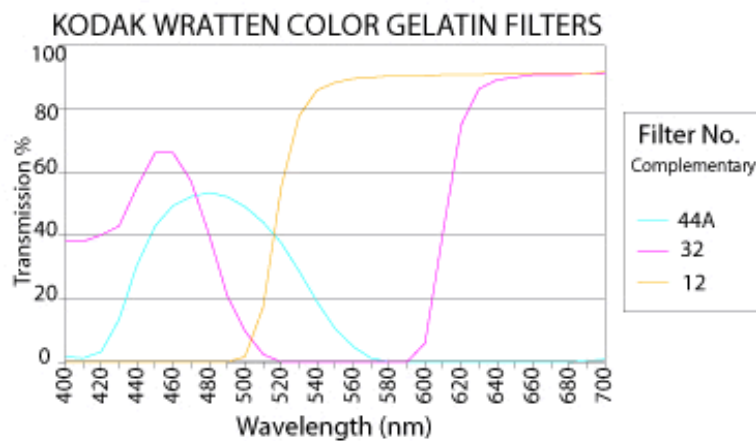
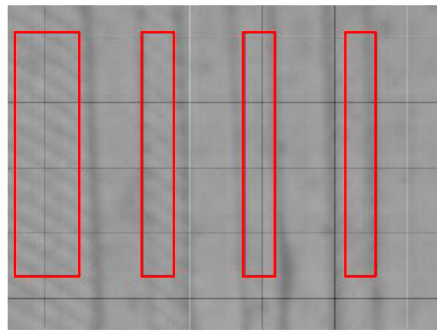
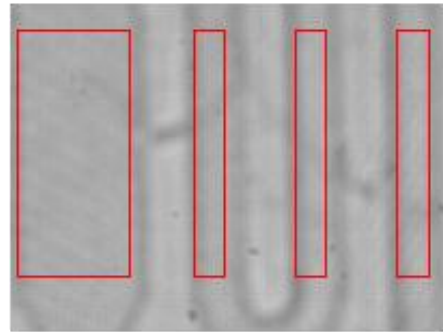


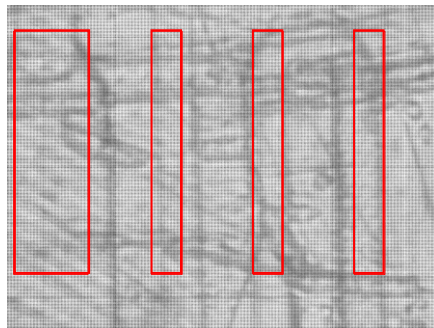
Figure 33: Transmission vs. Wavelength for Wratten 12 Filter



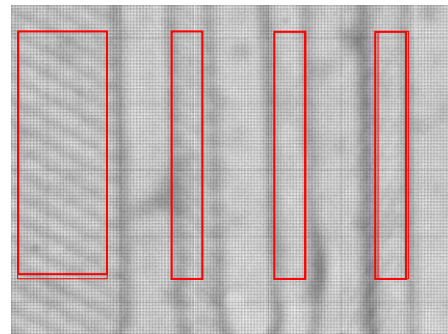
607 nm Bandpass Filter



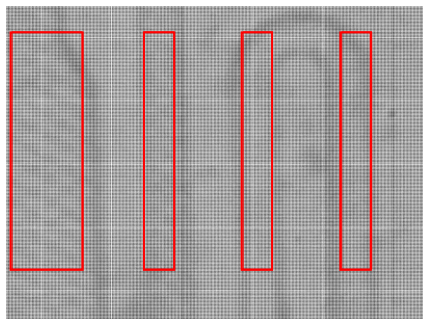
532 nm Bandpass Filter



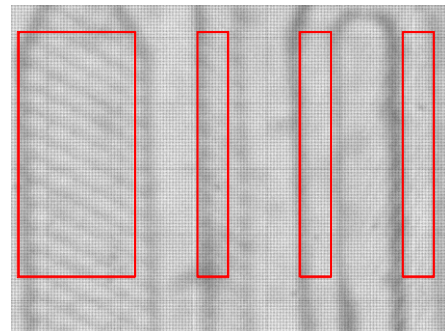
Kodak 12 Wratten Filter



Square Bandpass Filter



483 nm Bandpass Filter



500 nm Longpass Filter

Figure 34: Results for Cool White LED with various filters

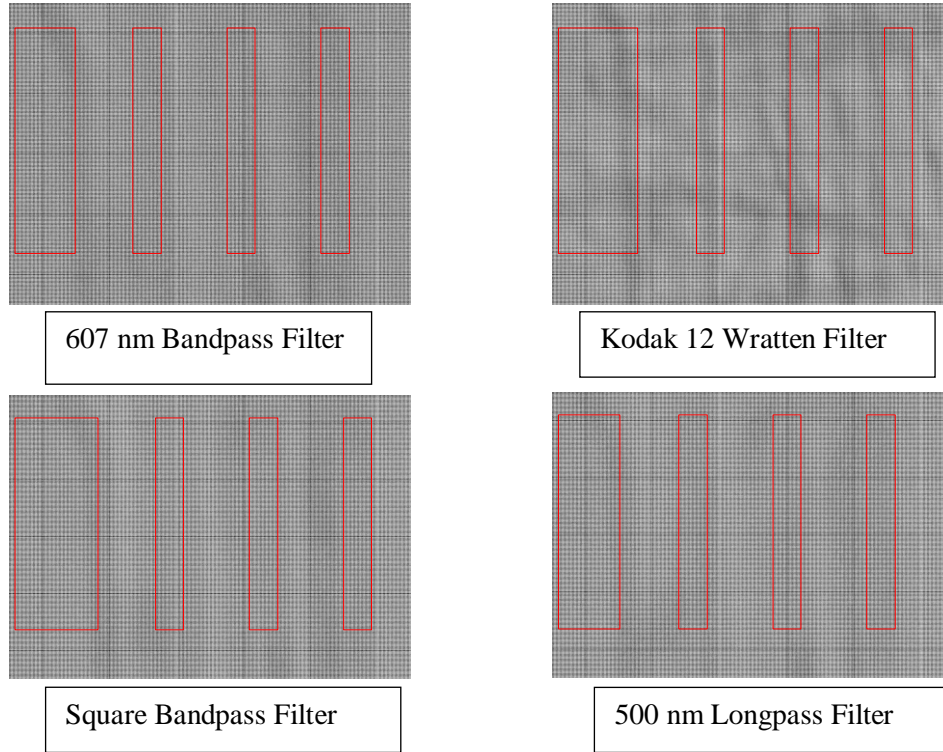


Figure 35: Flat Amber LED with different Filters

	Red	Blue	Amber	White	Cool White	UV	Green	Yellow	Flat Amber
607 bandpass Filter	X	X	X	X	✓	✓	X	X	✓
532 10fwhm Wratten no 12	X	X	X	X	✓	X	X	X	X
Square bandpass filter	X	✓	X	X	✓	X	X	X	✓
483 bandpass w 31 nm	X	X	X	✓	✓	X	X	X	✓
500 nm Longpass	X	X	X	X	✓	X	X	X	✓

Table 8: Results of using different LEDs with different filters

4.1.4 Height and Voltage of LED

Another study varied the voltage and the height of the LED from the detection site to determine the optimum height and voltage. The two LEDs that were chosen for this test were the Amber LED and the Cool White LED. Table 9 shows the results from the Amber LED while Table 10 shows the results from the cool white LED. In both of these tables, a “X” denotes that the edges were not able to be established and a “✓” means the edge detection and pumping algorithms worked. Looking at these two tables, it is clear that the LED has to be a certain distance from the detection site for the image to be able to detect the edges and work with the feedback pumping. The Amber LED was not able to find any of the edges regardless of the setup. When the Amber LED was able to determine the edges previously with the various filters, it was located higher than 30mm from the detection site and the voltage the Arduino supplied was also higher. Image results from the Amber LED are not shown since they are completely black images.

The cool white LED was able to determine the edges after the LED was a height of at least 20mm from the top of the PDMS chip. At distances of 25mm and 30mm, the picture that was taken from the CCD imager became clearer. These images are shown in Figure 36. This test shows that the farther away from the chip that the LED is, the better the image will be. The distance that the LED is limited to in the actual unit is 27.5mm because of the height of the cover. These results prove that in the actual handheld unit, the distance that the LED will be at will be able to produce an acceptable image for edge detection and the feedback pumping.

Amber LED	5mm	10mm	15mm	20mm	25mm	30mm
1.6V	X	X	X	X	X	X
2V	X	X	X	X	X	X
2.4V	X	X	X	X	X	X
2.8V	X	X	X	X	X	X

Table 9: Results of Voltages and Heights for the Flat Amber LED

White LED	5mm	10mm	15mm	20mm	25mm	30mm
2.4V	X	X	X	✓	✓	✓
2.6V	X	X	X	✓	✓	✓
2.8V	X	X	X	✓	✓	✓

Table 10: Results of Voltages and Heights for the White LED

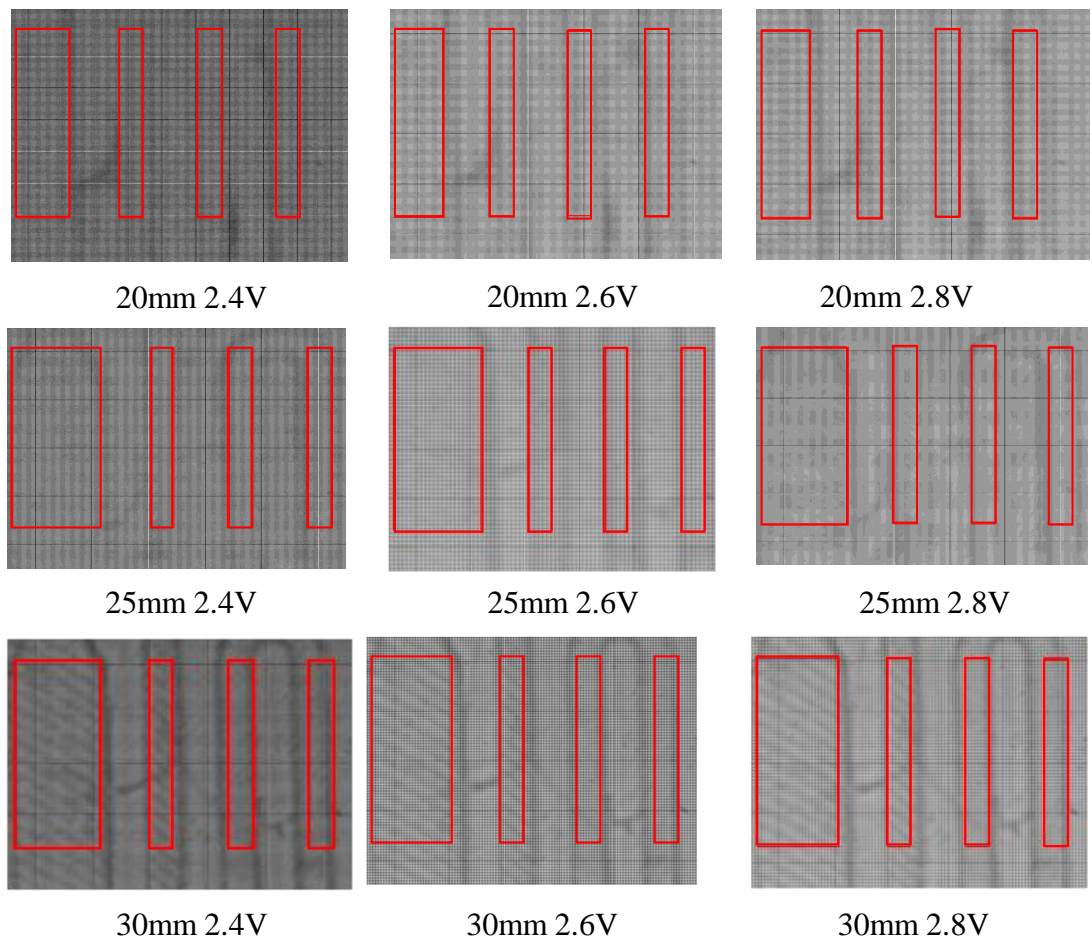


Figure 36: Image results for white LED at various voltages and heights

4.1.5 Feedback Pumping

Manually pumping the liquid in the microfluidic channel, it is shown that the feedback controller is working and is able to distinguish liquid from air. Figure 37 shows the controller in use with a white area representing liquid in the channel and a black area representing air. This figure shows that liquid is being pumped out of the detection site and then pumped back in with MATLAB is waiting 0.5 seconds before

taking each image. Additionally a pump connected to the microcontroller but not to the chip would turn on and off at the appropriate time.

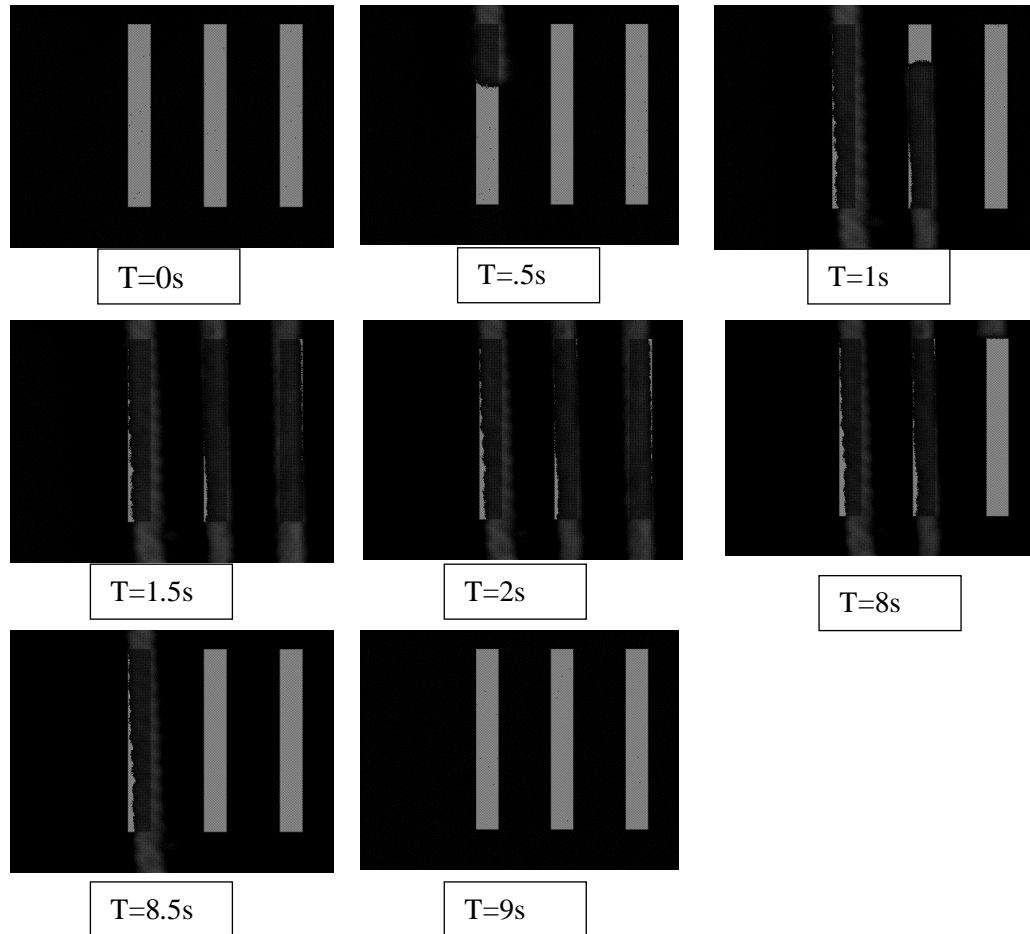


Figure 37: Manual Pumping with half second delay

Obtaining the volumetric flow rate is desirable to see how fast the pump was actually pumping. Varying the duration of pause command in MATLAB (0.5 seconds to 0 seconds) did not prove that useful because the fastest that MATLAB was able to take images during the feedback controller was ~ 0.2 seconds. At ~ 0.2 seconds, the feedback controller was still taking images too slowly and the liquid was pumping too fast to determine a true flow rate even if a $10\mu m$ orifice was used. Instead, an

approximate flow rate could be determined. The fastest that a CCD can take an image with MATLAB is dependent on the amount of random access memory (RAM) that the computer has. On a computer running Windows 7 with 4GB of RAM, the fastest an image could be taken is every 0.25 seconds and on a computer running Windows 7 with 8 GB of RAM this is every 0.19 seconds. If a $4\mu\text{m}$ orifice was used, then the liquid would not be able to pump at all. The $4\mu\text{m}$ orifice may not have worked since liquid had been previously introduced to it in another experiment. Since the hole of the orifice is so small any contact with liquid will completely block the orifice.

By visual inspection, it could be seen that the $10\mu\text{m}$ orifice significantly slowed down the flow rate of the liquid compared to when no orifice was used. Even though the images were taken too slowly to determine the flow rate, this controller still is able to work with a sequentially loaded chip because the volume of reagents that are in the chip are much greater than the volume of the detection site. These images of the detection site with liquid and air using a $10\mu\text{m}$ orifice are shown in Figure 38.

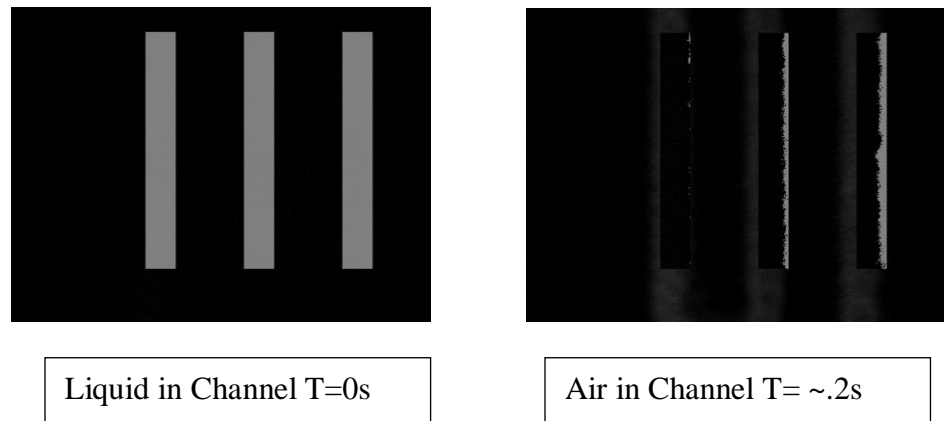


Figure 38: Pumping with Bartels Micropump

The total volume of the 'S' channel is given by Equation (2) where L is length, W is width, H is depth of the channel, r_o is the outer radius and r_i is the inner radius of the curve. The total volume of the channel is 0.724 mm^3 or $7.24 \times 10^{-4} \text{ cm}^3$ using the dimensions from Figure 39. The Fire-I CCD was able to take images every 0.19-0.25 seconds. Using Equation (3) where Q is the volumetric flowrate, V is volume, and t is time. Using the assumption the first image is taken right before air enters the channel and the second image is taken right after the last bit of liquid leaves the channel, a flow rate of at least 0.00289 to $0.00381 \text{ cm}^3/\text{s}$ could be determined. In reality, the flow rate of this system is higher but these flow rates represent the highest flow rate that could be captured with the CCD imager used.

$$(3(L*W) + \pi(r_o - r_i)^2)*H \quad (2)$$

$$Q = \frac{\Delta V}{\Delta t} \quad (3)$$

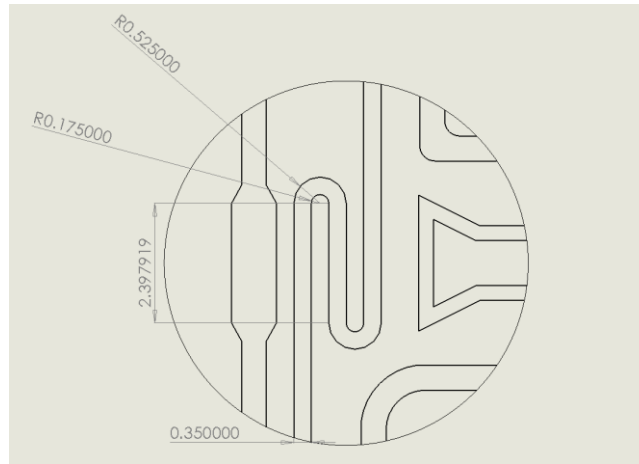


Figure 39: Dimensions of the 'S' channel 0.25mm height

A different approach to determining the flow rate was taken. The micropump was first hooked up to a PDMS chip without an orifice and a video was taken with an

iPhone. Then the pump was hooked up to a 10 μm orifice and a video was taken with an iPhone. The videos were then analyzed using Sony Vegas Pro 9.0. The values for the flow rate were $0.4755\text{cm}^3/\text{s}$ with no orifice and $0.007052\text{cm}^3/\text{s}$ with a 10 μm orifice. These numbers make sense since it is slightly higher than the flow rate obtained by the feedback controller using the Fire-I camera. These results are shown in Table 11.

	Volumetric Flow Rate cm^3/s (mm^3/s)
Feedback Controller μm orifice	0.00289 to 0.00381 (2.89 to 3.81)
iPhone video No orifice	0.4755 (475.5)
iPhone video 10 μm orifice	0.007052 (7.052)

Table 11: Results for determining volumetric flow rate

The volume of reagents that are put in a sequentially loaded chip are $7\mu\text{L}$ or 7mm^3 and the flow rate with a $10\mu\text{L}$ orifice is $7.052\text{mm}^3/\text{s}$. The frequency the slug of reagent is moving is 1.007 Hz. For reliability, the CCD should sample at least twice the maximum frequency or about every .5 seconds and the CCD is currently sampling at every .2 seconds.

The feedback controller was also used on a chip with different microchannel geometry; shown in Figure 40. The width of this channel is 0.3 mm which is a 14.3 % reduction of the size of the channel (.035mm) in the final chip design. For this test, a manual ROI was placed since the edge detection software is tailored for the detection chamber and the ‘S’ channels. The edge detection software could be easily modified for different designs. To allow for different designs, the parameters in the program that would have to be changed are the edge or geometry that the program is looking that is considered a first edge, the number of ROIs, and the distance between the ROIs. The

controller was able to see a difference between fluid and air using this chip and turn on and off a pump accordingly.

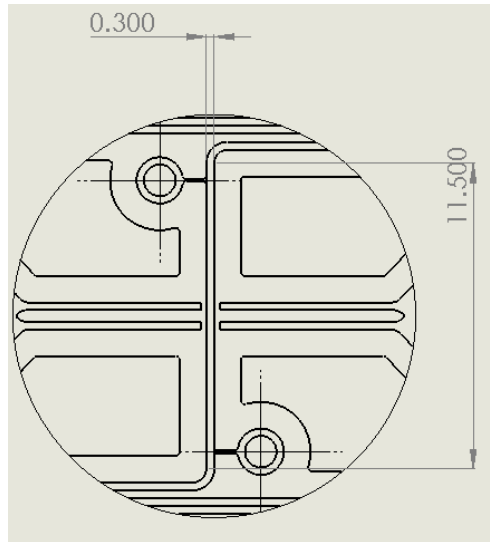


Figure 40: Different geometric chip design (depth 0.25mm)

Various liquid and biological reagents were tested to make sure the feedback controls will work when they are introduced to the system. The majority of these liquids had a clear appearance with a few exceptions; the whole blood and serum and quantum dots. The serum had a yellow tint to it while the whole blood was very dark. However to the CCD imager, the yellow tint did not matter as the feedback was able to detect the serums presence or lack thereof as shown in Figure 41.

When the whole blood was introduced to the channel, the channel got significantly darker. This means that the program could easily be modified to respond to the whole blood by looking for a darker image when fluid is in the channel rather than a lighter one. Whole blood in a channel is shown in Figure 42. The fact that whole blood does not work with the way the feedback controller is currently set up is

not bad because whole blood should never be introduced to the system. The whole blood will be filtered to serum before it can enter the chip.

The other liquid that was of interest was the various concentrations of quantum dots. Since the quantum dots are excited at 405nm and white light is composed of all wavelengths of visible light, the quantum dots will naturally fluoresce. This did not prove to be a problem during the pumping and the feedback control was able to accurately determine when there was a fluid in the chamber or not. Quantum dots in the channel are shown in Figure 43. The pumping of different concentrations of quantum dots would be used in the calibration chamber during the actual test. The fluids that work and the fluid that don't work with the feedback controller are shown in Figure 44.



Figure 41: Serum in Feedback Loop

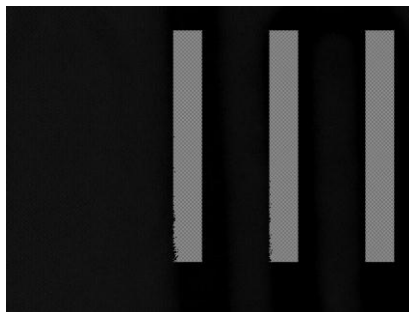


Figure 42: Whole Blood in Detection Channel



Figure 43: Quantum Dots in Detection Channel

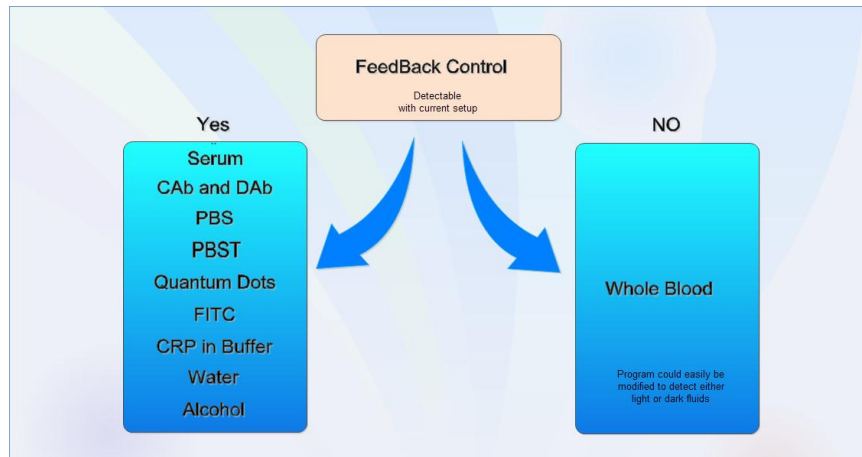


Figure 44: List of different Fluid that work with feedback control

4.2 Smartphone Integration

4.2.1 Microcontroller Prototypes

The initial Arduino prototype that was constructed is shown in Figure 45. This prototype featured an Arduino Mega connected to a Wifi Shield and TouchShield Stealth. This prototype was important because it showed that it was possible to control the unit both wirelessly and with a touchscreen. An Arduino Mega needed to be used since it has multiple serial inputs which are necessary to control the WiFi Shield and the TouchShield at the same time. Eventually, a unit could be constructed without a touchscreen and just use the smartphone app as a GUI.



Figure 45: Initial handheld unit prototype

The final microcontroller that was used in the handheld unit with wireless capabilities is shown in Figure 46. This is an Arduino Nano Mega 2560 that is connected with a Wifi Shield and a Touchscreen Slide. The Arduino Nano Mega is a smaller version of the original Arduino Mega. The hardware modifications which are the jumper wires can be seen in the image below. The final handheld unit that was produced is shown in Figure 47.

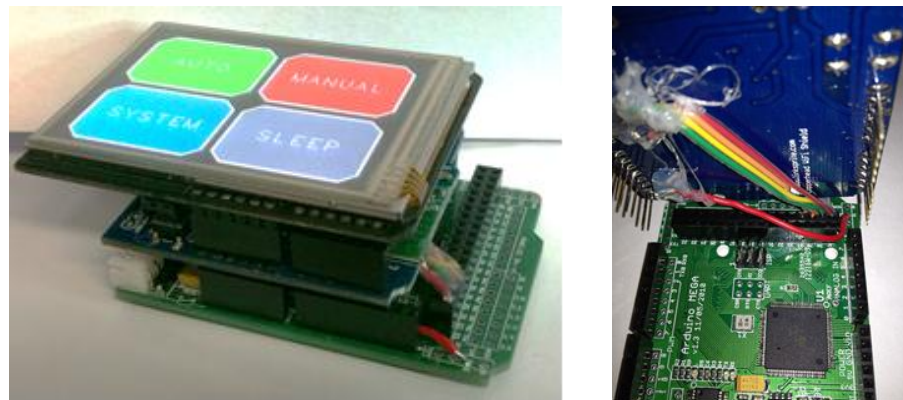


Figure 46: Final Microcontroller and modifications



Figure 47: Prototype of the Handheld unit

4.2.2 Smartphone Applications

The first generation of the smartphone app is shown in Figure 48. The app icon is circled on the image to the left and the actual app is shown on the right. The purpose of this smartphone app was to show that complete control over an Arduino microcontroller could be achieved. If the button called 'LED on' was pressed or the button called 'Pump on' was pressed, two different LEDs would be able to light up. The app was able to stay on the same screen because a UIWebView that was hidden was called on the button press. This app was tested on a 4g iPod Touch as well as an iPhone 3GS.

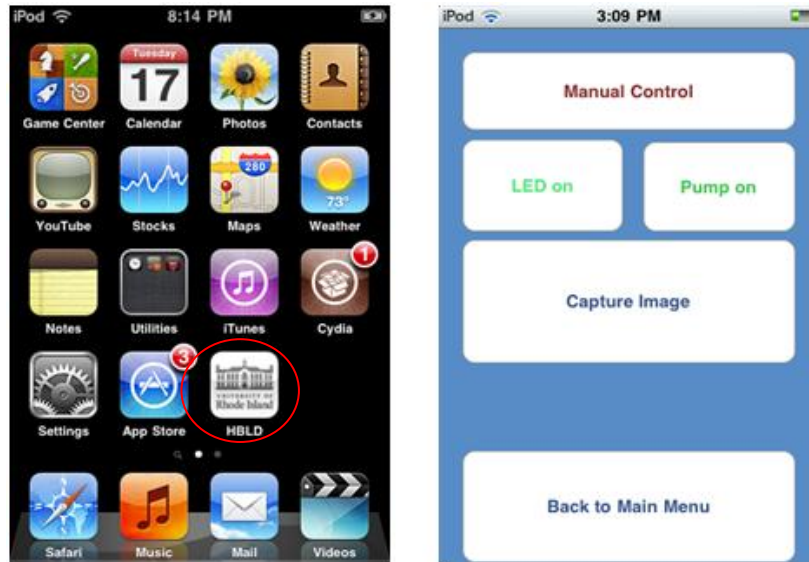


Figure 48: First generation of smartphone app on iPhone

The second generation of smartphone apps consisted of an Android app that had multiple tabs. One of these tabs allowed the user to input information, choose the test that was desired and start a test. The other screen allowed for the results to be sent to the phone when the button was pushed. The designs of both of these screens are shown in Figure 49. The information that could be entered was a patient's name, birthday (from which their age could be determined), gender, an email to send results from and the corresponding password, and an email to send the results too. One of the drawbacks of this android app is that the tests and people were not saved. This caused a loss of inputted data after the app was closed and the patient's information would have to be entered again as well as information that wouldn't change such as the email the results are sent from and password.

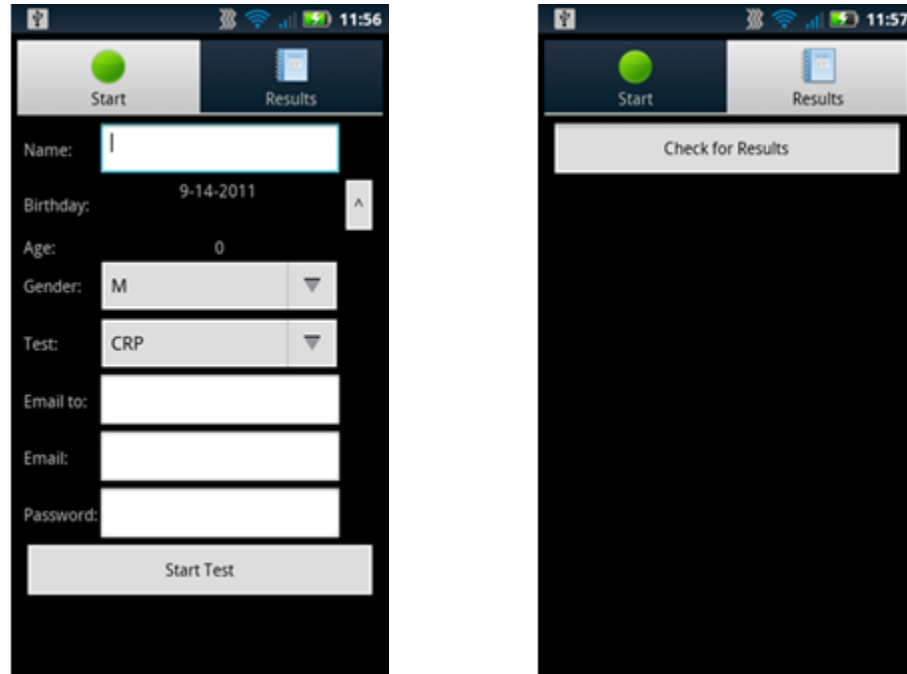


Figure 49: Second Generation of smartphone app on Android

The third generation of smart phone apps is the most recent and the app was created for the iPhone. This iPhone app now has the ability to add, store, and delete patient information. This patient directory is stored in a plist so if the iPhone goes to the main screen, then the information that is stored will not be lost. This app has three tabs which are shown Figure 50.

These tabs are for inputting user information, getting test results, and using the manual controls and adjusting settings. The manual control screen is labeled a.) in Figure 50. This figure shows the manual control setup and the different settings that can be edited. The settings that can be adjusted are the email that the tests results will be sent to, the email the tests results are sent from, password for the email, and server information.

The ability to change the IP address of the server is a new feature of this generation. Previously, the server IP address would have to be reloaded on the phone from the source code whenever it changed across the various networks. All of these variables that can be saved are stored in a plist called NSUserDefaults. This is a way to store and share data over multiple tabs easily. In Figure 50 images b, c, and d show the patient list, how the patient list is editable, and what the patient list looks like when a new patient is added. Image e shows what the Add patient screen looks like and image f shows what the screen looks like when a patient from the patient list is selected.

On the Add patient screen, the same information that could be added in the Android app can be added in this app. On the patient information screen the user will have the ability to choose the test that they want to run as well as look at information from the patient. If no test is selected, the app will not send the data and instead notify the user that they need to select a valid test in order to start a test.

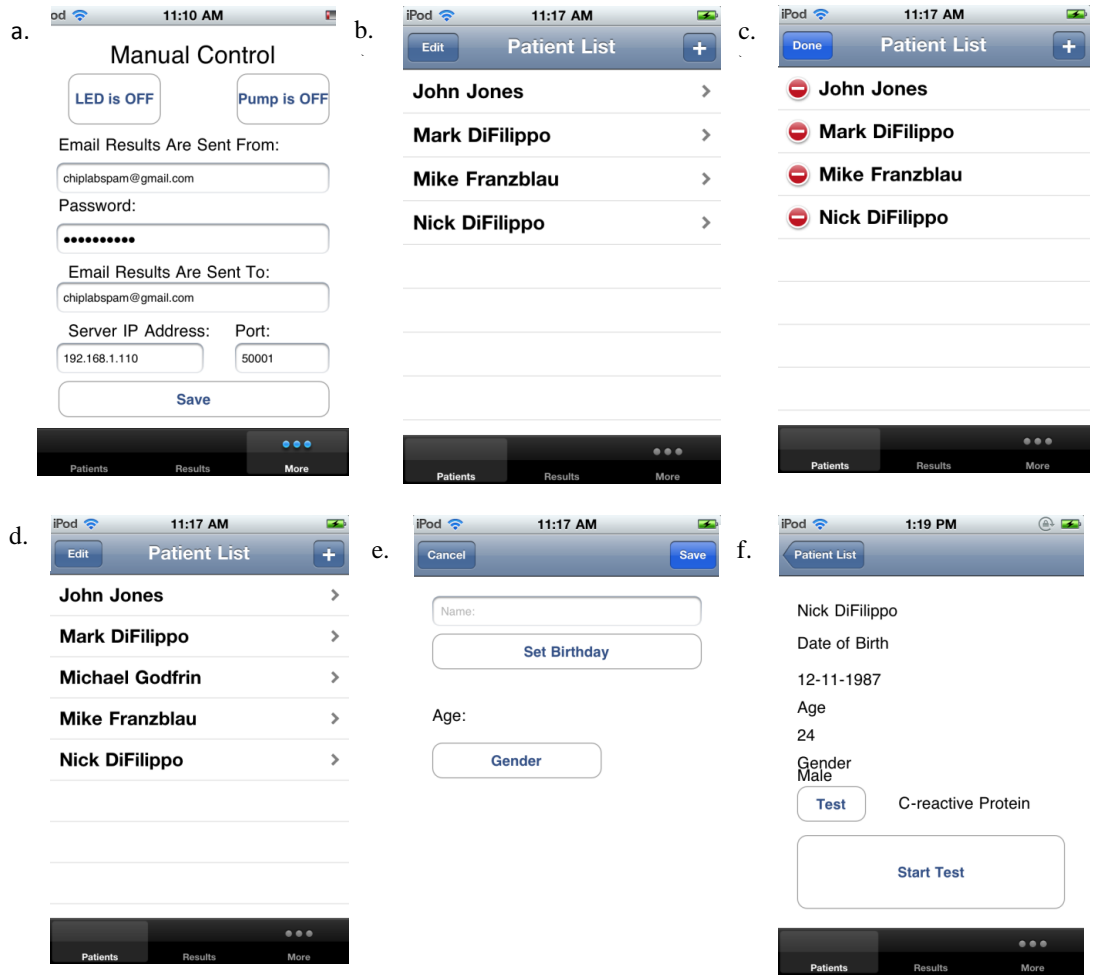


Figure 50: Third and Final Generation of smartphone app on iPhone

4.2.3 Network Integration

A server that is based on a remote computer can be listening on a certain port for a connection to be made from the smartphone app. When the connection is made, the patient information that was entered into the app will be transferred to the server. This will either be the Python server running the Twisted engine for the iPhone app or a Java Server for the Android app. After the server receives the message, it will call a Python script that will start the test on the microcontroller. If the microcontroller is called directly from the Android app, it will sometimes receive this command twice,

while the iPhone App will only send it once. To fix this problem, a Python script was used to start the test instead of directly calling the microcontroller from the smartphone app.

After the test has been started, the microcontroller will make a connection with a different Python server at the appropriate times. This server will start MATLAB when called and run the detection algorithm or feedback pumping script at startup. MATLAB will then be able to update the text (txt) file that the Results tab so the smartphone app can see the progress of the test. After the main detection program in the MATLAB has finished analyzing the images, MATLAB will call a Python script that will be able to send an email to the specified email address and the app will also be able to receive the test results. If an external IP address, instead of an internal IP address was used, it would be possible to control and start this test from anyplace that has access to a wireless network.

4.2.4 Preliminary Communication for a Completely Wireless Unit

Work has also been done on a preliminary network loop for a completely wireless unit. This unit could use a FEZ Cobra microcontroller by GHI Electronics and costs \$150. This microcontroller is based on the EMX module and has 4.5 megabytes (MB) of flash memory and 16 MB of RAM. The FEZ Cobra with a webcam and wireless unit is shown in Figure 52. The proposed network loop that includes sending images is shown in Figure 53. This communication loop was constructed and images were sent wirelessly; however it was not possible to run a test since the webcam used did not send data in a raw format. Using the FEZ Cobra, it was possible to send an image across the network to a Python script that was listening and

waiting for the image. Figure 51 shows the amount of time it takes in seconds to send different amount of bytes with the WiFi unit that is used. The linear fit has a coefficient of determination R^2 value of .99802.

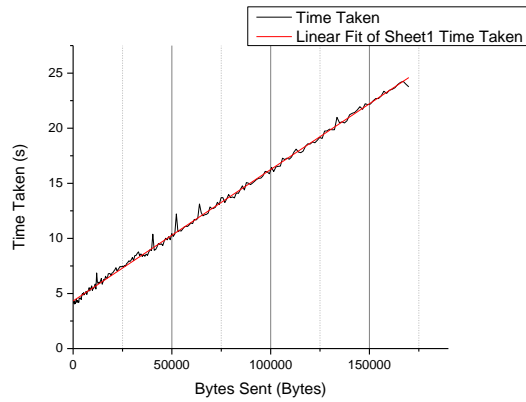


Figure 51: Time taken to send bytes wirelessly from microcontroller



Figure 52: Fez Cobra

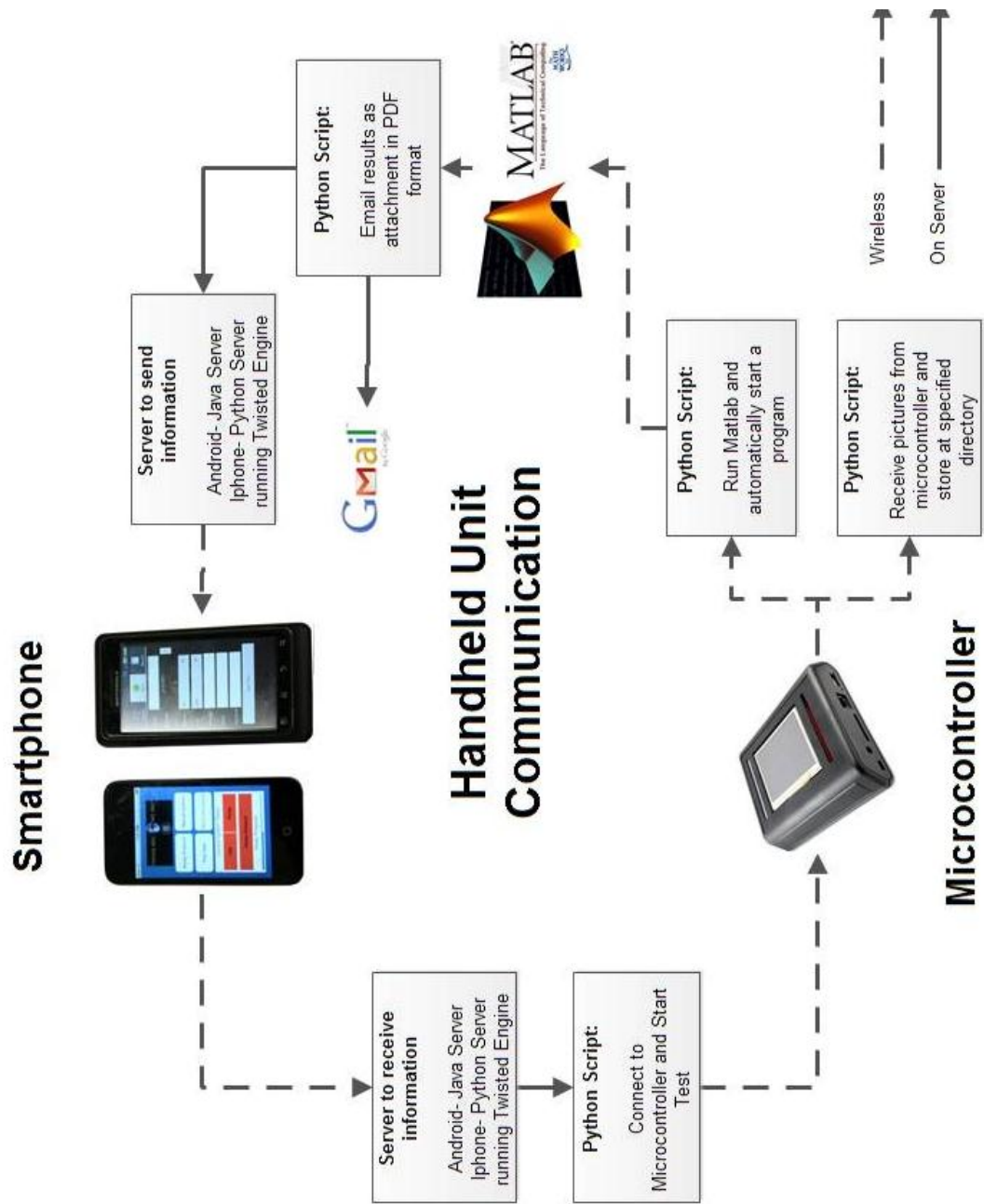


Figure 53: Proposed Network Communication for a completely wireless unit

CHAPTER 5 - CONCLUSION

5.1 Conclusions

A fluid handling system was created that was able to determine the edges and accurately place ROI inside the channels of a microfluidic chip using a custom edge detection method. This system was also able to distinguish when liquid or air was in the channels and turn a pump on or off accordingly. This increased the reliability of the pumping for a sequentially loaded chip.

A custom iPhone app was created that was able to send data to a central server and start a test on a handheld microfluidic unit. The microfluidic unit could then communicate with the server and MATLAB when appropriate. During and at the end of the test, the iPhone app would be able to receive the results of the test. This wireless communication system that was introduced, would be able to perform an automated test for CRP.

5.2 Future Work

The ability to make a completely wireless unit is still a challenge that exists. One of the limitations of the unit today is the CCD that is used. The CCD requires a driver that needs to be installed and a Fire Wire cable that needs to be hooked up to a computer. This is the only inexpensive raw CCD imager that is on the market- which is the reason it was used for this project. Unfortunately this webcam cannot be hooked up to the FEZ Cobra because it requires drivers. If a driverless CCD imager that could

be hooked up to the FEZ Cobra is manufactured, then the communication loop that is shown in Figure 53 could be used.

A different way of performing the feedback control would also have to be implemented. Since the CCD would no longer be hooked up to the computer, the feedback controller would not be able to operate close to real time since images would have to be sent wirelessly. This is a huge amount of information to send and process wirelessly. One way to perform the pumping would be to have the pump turn on for a specified amount of time, turn off and then send an image to MATLAB for analysis. The MATLAB analysis would then send back to the microcontroller whether a change had occurred in the ROI or not. If a change had occurred then the pump could stay off and if a change did not occur then the pump could turn on again for a specified amount of time.

Another way of performing a test with a CCD imager would be to completely eliminate the need to send the images wirelessly. This would require a microprocessor that is powerful enough to perform on board image processing. The FEZ cobra may be able to perform these tasks or an even more powerful unit could be used such as the Raspberry Pi 35. This is a mini computer that is sold for \$25-35 and has 256MB of RAM.

A third way would be to change the equipment used for detection and incorporate a photodiode that would be able to get an analog voltage that could determine when there was liquid or air in the detection chamber since the amount of light that enters the photodiode would change. Alternatively, quantum dots; producing different fluorescent lights could be inserted in the different reagents. As these

different reagents enter the detection site, a UV light could excite the quantum dots producing different fluorescent lights in order to verify the right reagent has reached the detection site.

During the feedback control it may be beneficial to extend the controller to work if blood is in the channel. Even though whole blood should never be introduced into the PDMS chip, it could be possible to check if whole blood was present as a way to detect a potential problem. If there was whole blood present then the server could send a command to the microcontroller that an error had occurred and needs to be addressed.

This idea of a communication loop could be extended to many different areas especially paper microfluidics. It would be possible to take a picture of a detection site of a paper microfluidic chip with a smartphone app and send the results to a computer or the smartphone itself to be analyzed. The results of this test would also be able to be emailed or sent back to a smartphone.

NOMENCLATURE

ADC	Analog to digital converter
App	Smartphone application
APOCIS	Affordable Point of Care ImmunoAssay System
BSA	Bovine Serum Albumin
bit	Binary digit
CCD	Charge-coupled device
CMOS	Complementary metal-oxide semiconductor
CRP	C-reactive protein
ELISA	Enzyme-linked immunosorbent assay
FITC	Fluorescein isothiocyanate
FEZ	Fast and Easy
FTP	File Transfer Protocol
FWHM	Full width half maximum
GUI	Graphics user interface
HbA1c	Glycosylated Hemoglobin
HE4	Human Epididymis protein
HM	Home Monitoring
HTTP	Hypertext transfer protocol
hsCRP	High Sensitivity C-Reactive Protein
ISP	Internet Service Provider
JPEG	Joint Photographic Experts Group
LASER	Light amplification by stimulated emission of radiation

LED	Light emitting diode
LOC	Lab-on-Chip
MB	Megabyte
MISO	Master in slave out
MOSI	Master out slave in
NASA	National Aeronautics and Space Administration
PDMS	Polydimethylsiloxane
PEEK	Polyetheretherketone
POC	Point-of-Care
RAM	Random Access Memory
ROI	Region of Interest
SCL	System clock line
SCK	System clock
SS	Slave Select
SSH	Secure Shell Client
TE	Tris Ethylenediaminetetraacetic
TCP/IP	Transmission control protocol and internet protocol
TIFF	Tagged image file format
Txt	Text File
UDP	User datagram protocol
URI	University of Rhode Island
URL	Uniform Resource Locator
U.V.	Ultraviolet

BIBLIOGRAPHY

- [1] Schuyler Vowell. Microfluidics: The effects of surface tension. March 2009.
- [2] N.T. Nguyen and S.T. Wereley. *Fundamentals and applications of microfluidics*. Artech House Publishers, 2002.
- [3] G.M. Whitesides. The origins and the future of microfluidics. *Nature*, 442 (7101): 368–373, 2006.
- [4] C. Rivet, H. Lee, A. Hirsch, S. Hamilton, and H. Lu. Microfluidics for medical diagnostics and biosensors. *Chemical Engineering Science*, 66 (7): 1490–1507, 2011.
- [5] P.B. LUPPA, C. MÜLLER, A. SCHLICHTIGER, and H. SCHLEBUSCH. Point-of-care testing (poc): Current techniques and future perspectives. *TrAC. Trends in analytical chemistry*, 30 (6): 887–898, 2011.
- [6] CS Pattichis, E. Kyriacou, S. Voskarides, MS Pattichis, R. Istepanian, and C.N. Schizas. Wireless telemedicine systems: an overview. *Antennas and Propagation Magazine, IEEE*, 44 (2): 143–153, 2002.
- [7] W.G. Lee, Y.G. Kim, B.G. Chung, U. Demirci, and A. Khademhosseini. Nano/microfluidics for diagnosis of infectious diseases in developing countries. *Advanced drug delivery reviews*, 62 (4-5): 449–457, 2010.
- [8] C.D. Chin, V. Linder, and S.K. Sia. Lab-on-a-chip devices for global health: past studies and future opportunities. *Lab Chip*, 7 (1): 41–57, 2006.
- [9] C.D. Chin, T. Laksanasopin, Y.K. Cheung, D. Steinmiller, V. Linder, H. Parsa, J. Wang, H. Moore, R. Rouse, G. Umviligihozo, et al. Microfluidics-based

- diagnostics of infectious diseases in the developing world. *Nature Medicine*, 17 (8): 1015–1019, 2011.
- [10] P. Yager, T. Edwards, E. Fu, K. Helton, K. Nelson, M.R. Tam, and B.H. Weigl. Microfluidic diagnostic technologies for global public health. *NATURE-LONDON*-, 442 (7101): 412, 2006.
- [11] C.H. Ahn, J.W. Choi, G. Beaucage, J.H. Nevin, J.B. Lee, A. Puntambekar, and J.Y. Lee. Disposable smart lab on a chip for point-of-care clinical diagnostics. *Proceedings of the IEEE*, 92 (1): 154–173, 2004.
- [12] W.W. Chang, T.J. Sung, H.W. Huang, W.C. Hsu, C.W. Kuo, J.J. Chang, Y.T. Hou, Y.C. Lan, W.C. Kuo, Y.Y. Lin, et al. A smart medication system using wireless sensor network technologies. *Sensors and Actuators A: Physical*, 2011.
- [13] V. Shnayder, B. Chen, K. Lorincz, T.R.F. Fulford-Jones, and M. Welsh. Sensor networks for medical care. In *Proceedings of the 3rd international conference on Embedded networked sensor systems*, pages 314–314. ACM, 2005.
- [14] C.Y. Lee, C.L. Chang, Y.N. Wang, and L.M. Fu. Microfluidic mixing: A review. *International Journal of Molecular Sciences*, 12: 3263–3287, 2011.
- [15] R.H. Liu, M.A. Stremler, K.V. Sharp, M.G. Olsen, J.G. Santiago, R.J. Adrian, H. Aref, and D.J. Beebe. Passive mixing in a three-dimensional serpentine microchannel. *Microelectromechanical Systems, Journal of*, 9 (2): 190–197, 2000.

- [16] WK Schomburg and B. Scherrer. 3.5 μ m thin valves in titanium membranes. *Journal of Micromechanics and Microengineering*, 2: 184, 1992.
- [17] M.R. McNeely, A.R. Oliphant, and M.K. Spute. Fluid circuit components based upon passive fluid dynamics, October 2 2001. US Patent 6,296,020.
- [18] Y.C. Su, L. Lin, and A.P. Pisano. A water-powered osmotic microactuator. *Microelectromechanical Systems, Journal of*, 11 (6): 736–742, 2002.
- [19] G.M. Walker and D.J. Beebe. A passive pumping method for microfluidic devices. *Lab Chip*, 2 (3): 131–134, 2002.
- [20] V. Linder and D. Steinmiller. Flow control in microfluidic systems, April 22 2009. US Patent App. 12/428,372.
- [21] D.B. Weibel, M. Kruithof, S. Potenta, S.K. Sia, A. Lee, and G.M. Whitesides. Torque-actuated valves for microfluidics. *Analytical chemistry*, 77 (15): 4726–4733, 2005.
- [22] G. Zhang, W. Du, B.F. Liu, H. Hisamoto, and S. Terabe. Characterization of electrokinetic gating valve in microfluidic channels. *Analytica chimica acta*, 584 (1): 129–135, 2007.
- [23] K. Hosokawa and R. Maeda. A pneumatically-actuated three-way microvalve fabricated with polydimethylsiloxane using the membrane transfer technique. *Journal of micromechanics and microengineering*, 10: 415, 2000.
- [24] A.K. Au, H. Lai, B.R. Utela, and A. Folch. Microvalves and micropumps for biomems. *Micromachines*, 2 (2): 179–220, 2011.

- [25] M.A. Unger, H.P. Chou, T. Thorsen, A. Scherer, and S.R. Quake. Monolithic microfabricated valves and pumps by multilayer soft lithography. *Science*, 288 (5463): 113–116, 2000.
- [26] P. Griss, H. Andersson, and G. Stemme. Expandable microspheres for the handling of liquids. *Lab Chip*, 2 (2): 117–120, 2002.
- [27] A.K. Henning, M. Zdeblick, J.S. Fitch, D.A. Hopkins Jr, and L.J. Lilly. Low-power thermopneumatic microvalve, October 10 2000. US Patent 6,129,331.
- [28] A. Wego, H.W. Glock, L. Pagel, and S. Richter. Investigations on thermopneumatic volume actuators based on pcb technology. *Sensors and Actuators A: Physical*, 93 (2): 95–102, 2001.
- [29] H. Takao, K. Miyamura, H. Ebi, M. Ashiki, K. Sawada, and M. Ishida. A mems microvalve with pdms diaphragm and two-chamber configuration of thermo-pneumatic actuator for integrated blood test system on silicon. *Sensors and Actuators A: Physical*, 119 (2): 468–475, 2005.
- [30] D. Litwiller. Ccd vs. cmos: Facts and fiction, reprinted from the jan. 2001 issue of photonics spectra© laurin publishing co. *Inc.*(4 pgs).
- [31] H.T. HYTTI. Characterization of digital image noise properties based on raw data. In *Proceedings of SPIE, the International Society for Optical Engineering*, pages 60590A–1. Society of Photo-Optical Instrumentation Engineers, 2006.
- [32] S.J. Moon, H.O. Keles, Y.G. Kim, D. Kuritzkes, and U. Demirci. Lensless imaging for point-of-care testing. In *Engineering in Medicine and Biology*

- Society, 2009. EMBC 2009. Annual International Conference of the IEEE,* pages 6376–6379. IEEE, 2009.
- [33] S.J. Moon, H.O. Keles, A. Ozcan, A. Khademhosseini, E. Hægstrom, D. Kuritzkes, and U. Demirci. Integrating microfluidics and lensless imaging for point-of-care testing. *Biosensors and Bioelectronics*, 24 (11): 3208–3214, 2009.
- [34] S. Seo, T.W. Su, D.K. Tseng, A. Erlinger, and A. Ozcan. Lensfree holographic imaging for on-chip cytometry and diagnostics. *Lab Chip*, 9 (6): 777–787, 2009.
- [35] S. Seo, S.O. Isikman, I. Sencan, O. Mudanyali, T.W. Su, W. Bishara, A. Erlinger, and A. Ozcan. High-throughput lens-free blood analysis on a chip. *Analytical chemistry*, 82 (11): 4621–4627, 2010.
- [36] J. Balsam, M. Ossandon, Y. Kostov, H.A. Bruck, and A. Rasooly. Lensless ccd-based fluorometer using a micromachined optical söllner collimator. *Lab Chip*, 11 (5): 941–949, 2011.
- [37] A. Roda, M. Mirasoli, L.S. Dolci, A. Buragina, F. Bonvicini, P. Simoni, and M. Guardigli. Portable device based on chemiluminescence lensless imaging for personalized diagnostics through multiplex bioanalysis. *Analytical Chemistry*, 2011.
- [38] A.F. Coskun, T.W. Su, and A. Ozcan. Wide field-of-view lens-free fluorescent imaging on a chip. *Lab Chip*, 10 (7): 824–827, 2010.
- [39] J. Reichman. Handbook of optical filters for fluorescence microscopy. *Chroma Technology Corporation*, 2000.

- [40] J. Canny. A computational approach to edge detection. *Pattern Analysis and Machine Intelligence, IEEE Transactions on*, (6): 679–698, 1986.
- [41] A.C. Bovik. *Handbook of image and video processing*. Academic Press, 2005.
- [42] E. Nadernejad, S. Sharifzadeh, and H. Hassanpour. Edge detection techniques: Evaluations and comparisons. *Applied Mathematical Sciences*, 2 (31): 1507–1520, 2008.
- [43] R. Maini and H. Aggarwal. Study and comparison of various image edge detection techniques. *International Journal of Image Processing (IJIP)*, 3 (1): 1, 2009.
- [44] Transmission control protocol tcp. [http://technet.microsoft.com/en-us/library/cc756754\(v=ws.10\).aspx](http://technet.microsoft.com/en-us/library/cc756754(v=ws.10).aspx), accessed on June 12, 2012.
- [45] The tcp/ip model. [http://technet.microsoft.com/en-us/library/cc786900\(v=ws.10\).aspx](http://technet.microsoft.com/en-us/library/cc786900(v=ws.10).aspx), accessed on June 12, 2012.
- [46] G. Huston. Ipv4-how long do we have? 2003.
- [47] M. Jouaneh. *Fundamentals of Mechatronics*. CL Engineering, 2011.
- [48] J.S. Choi, B. Yi, J.H. Park, K. Choi, J. Jung, S.W. Park, and P.L. Rhee. The uses of the smartphone for doctors: An empirical study from samsung medical center. *Healthcare informatics research*, 17 (2): 131, 2011.
- [49] Apple Inc. Doylestown hospital. <http://www.apple.com/iphone/business/profiles/doylestown/>, accessed on January 30, 2012.

- [50] Apple Inc. Mount Sinai hospital.
<http://www.apple.com/iphone/business/profiles/mt-sinai/>, accessed on January 30, 2012.
- [51] J. Sarasohn-Kahn and California HealthCare Foundation. *How smartphones are changing health care for consumers and providers*. California HealthCare Foundation, 2010.
- [52] C. Paton and M. Al-Ubaydli. The doctor's pda and smartphone handbook: medical records. *JRSM*, 99 (4): 183–184, 2006.
- [53] B.M. Dala-Ali, M.A. Lloyd, and Y. Al-Abed. The uses of the iPhone for surgeons. *The Surgeon*, 9 (1): 44–48, 2011.
- [54] O. Franko. Smartphone apps for orthopaedic surgeons. *Clinical Orthopaedics and Related Research*, 469 (7): 2042–2048, 2011.
- [55] J.K. Mankanjuola and M.F. Bultitude. Smartphone applications for the urology trainee. *BJU international*, 109 (2): E3–E4, 2012.
- [56] S. Patel, K. Lorincz, R. Hughes, N. Huggins, J. Growdon, D. Standaert, M. Akay, J. Dy, M. Welsh, and P. Bonato. Monitoring motor fluctuations in patients with parkinson's disease using wearable sensors. *Information Technology in Biomedicine, IEEE Transactions on*, 13 (6): 864–873, 2009.
- [57] S. Patel, K. Lorincz, R. Hughes, N. Huggins, J.H. Growdon, M. Welsh, and P. Bonato. Analysis of feature space for monitoring persons with parkinson's disease with application to a wireless wearable sensor system. In *Engineering in Medicine and Biology Society, 2007. EMBS 2007. 29th Annual International Conference of the IEEE*, pages 6290–6293. IEEE, 2007.

- [58] T.R.F. Fulford-Jones, G.Y. Wei, and M. Welsh. A portable, low-power, wireless two-lead ekg system. In *Engineering in Medicine and Biology Society, 2004. IEMBS'04. 26th Annual International Conference of the IEEE*, volume 1, pages 2141–2144. IEEE, 2004.
- [59] C. Park, P.H. Chou, Y. Bai, R. Matthews, and A. Hibbs. An ultra-wearable, wireless, low power ekg monitoring system. In *Biomedical Circuits and Systems Conference, 2006. BioCAS 2006. IEEE*, pages 241–244. IEEE, 2006.
- [60] D. Bansal, M. Khan, and A.K. Salhan. A computer based wireless system for online acquisition, monitoring and digital processing of ekg waveforms. *Computers in Biology and Medicine*, 39 (4): 361–367, 2009.
- [61] T. Gao, C. Pesto, L. Selavo, Y. Chen, J.G. Ko, J.H. Lim, A. Terzis, A. Watt, J. Jeng, B. Chen, et al. Wireless medical sensor networks in emergency response: Implementation and pilot results. In *Technologies for Homeland Security, 2008 IEEE Conference on*, pages 187–192. IEEE, 2008.
- [62] T. Gao, D. Greenspan, M. Welsh, R. Juang, and A. Alm. Vital signs monitoring and patient tracking over a wireless network. In *Engineering in Medicine and Biology Society, 2005. IEEE-EMBS 2005. 27th Annual International Conference of the*, pages 102–105. Ieee, 2006.
- [63] K. Lorincz, D.J. Malan, T.R.F. Fulford-Jones, A. Nawoj, A. Clavel, V. Shnayder, G. Mainland, M. Welsh, and S. Moulton. Sensor networks for emergency response: Challenges and opportunities. *Pervasive Computing, IEEE*, 3 (4): 16–23, 2004.

- [64] H. Choi, I.H. Park, H.G. Yoon, and H.M. Lee. Wireless patient monitoring system for patients with nasal obstruction. *Telemedicine and e-Health*, 17 (1): 46–49, 2011.
- [65] K.G. Ng, S.T. Wong, S.M. Lim, and Z. Goh. Evaluation of the cardi thermosensor wireless skin-contact thermometer against ear and axillary temperatures in children. *Journal of Pediatric Nursing*, 25 (3): 176–186, 2010.
- [66] W.D. van Marken Lichtenbelt, H.A.M. Daanen, L. Wouters, R. Fronczek, R.J.E.M. Raymann, N.M.W. Severens, and E.J.W. Van Someren. Evaluation of wireless determination of skin temperature using ibuttons. *Physiology & behavior*, 88 (4): 489–497, 2006.
- [67] S.Q. Wang, X. Zhao, I. Khimji, R. Akbas, W. Qiu, D. Edwards, D.W. Cramer, B. Ye, and U. Demirci. Integration of cell phone imaging with microchip elisa to detect ovarian cancer he4 biomarker in urine at the point-of-care. *Lab Chip*, 11 (20): 3411–3418, 2011.
- [68] L. Schwiebert, S.K.S. Gupta, and J. Weinmann. Research challenges in wireless networks of biomedical sensors. In *Proceedings of the 7th annual international conference on Mobile computing and networking*, pages 151–165. ACM, 2001.
- [69] R.P. Ricci, L. Morichelli, and M. Santini. Remote control of implanted devices through home monitoring™ technology improves detection and clinical management of atrial fibrillation. *Europace*, 11 (1): 54–61, 2009.
- [70] Henry Lin. Cell phone-based lateral flow assay for blood biomarker detection. NASA PROPOSAL NUMBER: 11-1 X13.01-9228.

- [71] John Dubach. Smart phone fluorescent chem8. NASA PROPOSAL NUMBER:11-1 X13.01-9659.
- [72] M. Faghri and P. Li. Development of a microfluidic fluorescence immunosensor for point-of-care diagnostics. In *Proceedings of the 2nd WSEAS international conference on Biomedical electronics and biomedical informatics*, pages 253–258. World Scientific and Engineering Academy and Society (WSEAS), 2009.
- [73] T.J. Clark, P.H. McPherson, and K.F. Buechler. The triage cardiac panel: Cardiac markers for the triage system. *Point of Care*, 1 (1): 42, 2002.
- [74] i-stat portable handheld. <http://www.abbottpointofcare.com/Products-and-Services/iSTAT-Handheld.aspx>, accessed on January 12, 2012.
- [75] Banalyst. <http://www.rohm.com/products/banalyst/top.html>, accessed on January 12, 2012.
- [76] Diagnostic chips. <http://www.diagnosticchips.com/>, accessed on June, 5 2012.
- [77] D.J. You, K.J. Geshell, and J.Y. Yoon. Direct and sensitive detection of foodborne pathogens within fresh produce samples using a field-deployable handheld device. *Biosensors and Bioelectronics*, 2011.